Université catholique de Louvain

Faculté des Sciences
Département de Physique
Institut d'Astronomie et de Géophysique Georges Lemaître

Modeling the Impact of Aviation on Climate

Travail de fin d'études présenté par Andrew Ferrone en vue de l'obtention du grade de licencié en Sciences Physiques

Promoteur	Pr. J. P. van Ypersele
Lecteurs	Dr. P. Marbaix Dr. B. Matthews
Année académique	2005–2006

ABSTRAIT

Dues aux émissions durant leur vol de croisière, les avions perturbent les concentrations de dioxyde de carbone, d'ozone de méthane et d'aérosols. D'autant plus, ils produisent sous certaines conditions des lignes de condensations, qui peuvent accentuer l'étendue des nuages cirrus.

Le but de ce mémoire est d'estimer ces différents facteurs et d'évaluer leur impact en Europe. Pour ce faire de façon précise, il faudrait utiliser un modèle régional tridimensionnel, comme par exemple MAR. Vu le temps limité, il n'était pas possible de faire une analyse complète des processus avec ce genre de modèle. C'est la raison pour laquelle nous avons décidé d'utiliser un modèle unidimensionnel, qui est plus intéressant si on veut identifier les facteurs les plus importants pour des études plus précises ultérieures.

Bien que le modèle 1D n'inclut pas tous les paramètres de rétroactions nécessaires, il est très utile pour explorer la sensibilité des impacts de certains facteurs et pour calibrer des résultats d'études avec des modèles 3D. Vu l'utilisation d'un modèle 1D, on s'est concentré sur l'impact des gaz à effet de serre et des aérosols, pour lesquelles ce type de modèle est approprié. Les impacts sur les nuages cirrus ne sont donc pas évalués bien que des études montrent que leur effets sont le plus important.

Nos résultats ont montré que l'augmentation de la température de surface due à l'aviation est actuellement deux fois plus haute en Europe que la moyenne globale, dû aux densités de trafic aérien élevés. De tous les facteurs qui ont été calculés, l'ozone est le plus important. Ceci montre que, si on veux introduire l'aviation dans un schéma d'échange de quotas d'émissions, il faut tenir compte de tous les facteurs. Une proposition ne tenant compte que du CO_2, pourrait conduire à une production excessive d'ozone et de traits de condensation.

D'autre part les résultats ont montré aussi, qu'il faut être prudent de la façon dont on intègre dans le temps et dans l'espace, si on veut utiliser un index climatique dans un schéma d'échange d'émissions. En effet les durées de vie dans l'atmosphère des divers facteurs sont très différents (du siècle pour le CO_2à quelques heures pour les traits de condensation) et en plus leur répartition géographique est très inhomogène.

De plus nous avons calculé une prédiction pour l'an 2025, pour laquelle le double des émissions par rapport à 2002 a été prévue. En accord on observe aussi la double d'augmentation de la température de surface. Finalement nous avons encore pris en considérations les variations saisonnières de l'impact. Avec ce modèle simple nous avons déduit que les impacts considérés sont plus importants en juillet qu'en janvier, ce qui s'explique par l'intensité accrue du trafic aérien en été.

Ce modèle simple nous a donc permis d'obtenir des premiers résultats importants, mais lors de ce mémoire, nous avons aussi aperçu les limites d'un tel modèle et la nécessité, d'utiliser un modèle plus complexe comprenant des paramètres de rétroaction afin de faire des recherches supplémentaires.

I would like to thank J. P. van Ypersele, B. Matthews *as well as* P. Marbaix *for their assistance throughout the academic year, and the scientific rigor they imposed on this thesis. Furthermore I would like to thank my parents, who made my studies possible, for their patience and encouragement. Finally I would like to thank* J. Guerrero *for giving me the permission to use his photograph on the cover of this thesis.*

FOREWORD

Today airliners produce only around 3% of total carbon dioxide emitted by anthropogenic sources every year. But the fast growing of air traffic is not likely to stop, and [IPCC 99] predicated for their reference scenario that traffic in 2050 will be 6.4 times higher than it was 1990. This implies that the figure of 3% is to change drastically as the emissions of other sources are going to be reduced in the future. For different scenarios [IPCC 99] predicted that the aviation sector produces between 6.8 to 16.2% of global emitted CO_2 in 2050.

To prevent this to happen, passengers need to be motivated to use other means of transports. Expressed in carbon dioxide par passenger-km, short hauled flights are the most polluting with nearly 100 gC per passenger-km. These flights could be easily replaced by high-speed trains for example. But also long hauled flight are very polluting with a minimum of 35 gC per passenger-km.

But airliners do not only change climate by the emissions of carbon dioxide. Figure 1 shows that also the concentration of other greenhouse gases, like ozone and methane are perturbed. The most recent studies show that condensation trails (contrails), who can involve into cirrus clouds seem to have together the greatest impact on climate. All these factors will be explained and analyzed in detail in the first chapter of this thesis.

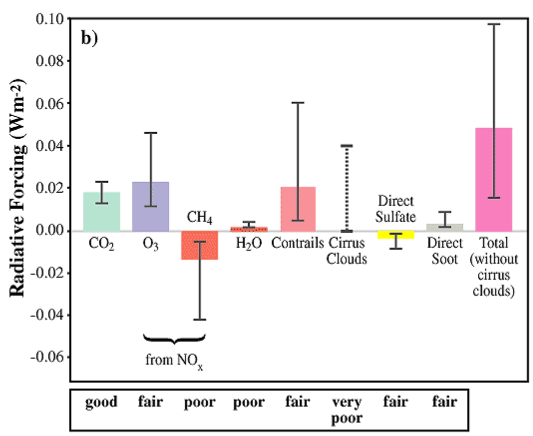

Figure 1: Radiative forcing from air traffic in 1992 from [IPCC 99] for the different impacts of aviation on climate

The aim of this thesis is to evaluate the relative impact of the different factors over Europe. As some of this forcing are local (ozone, contrails, cirrus clouds and aerosols) the highly inhomogeneous distribution of air traffic density over globe, implies that these factors are more important over Europe, where air traffic density is highest.

For this purpose a three dimensional model such as MAR would be state-of-the-art for a longer project, but it runs too slowly to complete analysis in time for this thesis. Another advantage of using a less complex one dimensional model is that sensitivity experiments can be performed more easily, and thus the fast running of the model is interesting to distinguish the impacts that need most attention for later studies. As we will discuss in section 1.4 there is also a need for a new index that quantifies the impact of aviation on climate. Different indexes can be compared more easily with a fast running one dimensional model, but this was not done in this thesis, due to time restrictions.

Although the 1D model misses many critical feedbacks, and also advection essential to understand regional climate, is can be used to explore sensitivity to various factors and to scale results from other 3D studies. Given that we use a 1D model it makes sense to focus on greenhouse gases and aerosols, for which this type of model is quite appropriate, rather than on cirrus (although chapter 1 shows that the latter effect is larger)

This work is divided into two parts. The first part includes chapter 1 to 3. As already mentioned, in chapter 1 we will give an overview and explanation of the different kinds of impacts of aviation on climate. This chapter is mainly based on [**IPCC 99**]; but there is an update with more recent articles which provided further insight since the IPCC publication in 1999. In chapter 2 we will discuss the technological and operational improvements that will affect the emissions of airliners in the next 25 to 50 years. The first part will be ended with chapter 3 which offers a description of the emission database AERO2k used to derive the results in the second part of my thesis. We will first explain how the data was obtained, then we will present the assumptions that were made to derive a forecast of emissions for 2025, and finally we will give the main uncertainties of the database.

In the second part we will present the modeling efforts that were made for this thesis as well as their results. In chapter 4 we will give a detailed description of the model that is used and we will also explain the changes that had to be done to this model in order to determine the climate impact of aviation in Europe. Finally, in chapter 5 we will give first some preliminary results which have been derived using the model. Next we will explain how we derived the changes in radiatively active substances, from the AERO2k emission database. Finally we will present the changes of surface temperature due to aviation in Europe in 2002 and 2025 that have been derived with the one dimensional model and discuss them.

At the end of the thesis the interested reader can find a description of the physics of atmospheric diffusion in Appendix A, and the technology of aircraft engines in appendix B.

TABLE OF CONTENTS

FIRST PART

Climate Change due to Aviation

CHAPTER I
POTENTIAL CLIMATE CHANGE DUE TO AVIATION

This chapter will give an overview of the impact of aviation on climate. To fully understand this impact, it begins by listing the main gases emitted by airliners. Section 1.1 then explains how these emissions are transformed in the plume behind the cruising airplane to changes in radiatively active substances. Finally the effect of these substances on climate change will be explained, including an order of magnitude estimate of their radiative forcing on the global mean.

Most of this chapter is based on [**IPCC 99**], but since scientific progress has been made since its publication, more recent insight into certain aspects has been included where necessary. These corrections can be found in [**Wit 04**] and the radiative forcing will also be updated to the ear 2002.

1.1 From Aircraft Emissions to Radiative Forcing

A detailed description of the gases emitted by aircraft engines is given in [**Brasseur 98**]. Only give a brief description of this topic will be given here.

Nearly all commercial aircrafts use kerosene as fuel. Kerosene designated as Jet A-1 is used nearly everywhere in the world except of the United States, where the common fuel is Jet A[1]. Jet fuels have to meet certain specifications all over the globe in order to assure the performance of the airplane, the safety of the passengers and to limit pollution (e.g. limitation of sulfur content). All jet fuels are composed primarily of hydrocarbons, with not more than 25% of aromatics. Furthermore olefins may be present, but their concentration is kept below about 1%. Sulfur concentration has to be below 0.3% by weight, and there may be trace levels of oxygenated organics. Finally metal contaminates such as iron, copper and zinc can be picked up from plumbing and storage systems, and be present in the low ppb range. As was noted by [**IPCC 99**], differences in jet fuel specifications around the world are relatively minor and have little effect on fleet exhaust emissions.

Under ideal conditions, combustion of kerosene produces carbon dioxide (CO_2) and water vapor (H_2O)(See figure 2). As kerosene contains also small amounts of sulfur (S), we also find sulfur dioxide (SO_2) in the exhaust products. The "real" combustion produces further gases. The second part of figure 2 illustrates the composition of the engine exhaust at cruise

[1] The main difference between Jet A-1 and Jet A is the maximum freezing point, which is $-40°$C for Jet A and $-47°$C for Jet A-1, achieved by addition of chemicals

conditions. We can see that combustion products only account for about 8.5% of the total mass going through the engine core. Of these products only about 0.4% is due to the non-ideal combustion process (soot, HC, and CO) and the oxidation of nitrogen (NO_x[2]).

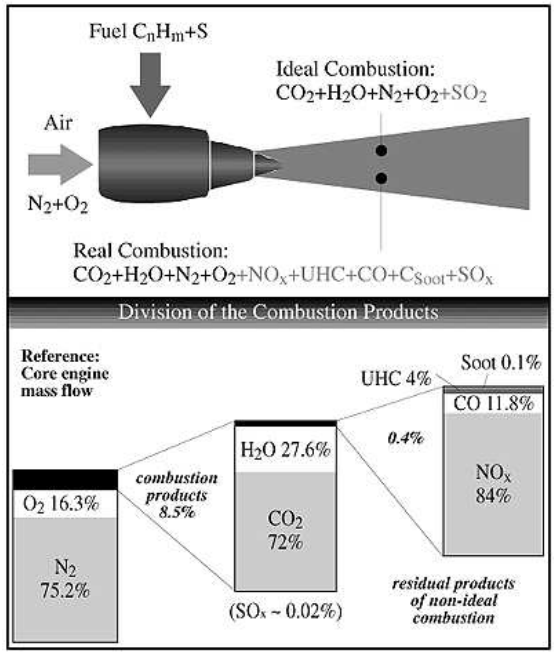

Figure 2: Schematic of ideal combustion products (top), and all existing combustion products, showing scale of each. (taken from [IPCC 99])

Furthermore aircraft engines emit aerosol particles and condensable gases, which lead to physical and chemical reactions in the plume of aircrafts. Details about these processes are not given here, but can be found in [IPCC 99] chapter 3 pp. 69–111. It should be noted that the main climatological impact of these emissions is a perturbed background in aerosol particles, and the formation of contrails, which both have an impact on natural cirrus clouds, as will be seen in section 1.2.

After these gases leave the engines they are further transformed by chemical reactions and micro-physical phenomena into radiatively active substances. These transformations are summarized in figure 3, and a short description will now be given. (More details can be found in [IPCC 99] chapters 2 and 3, pp. 28).

1.1.1 Impacts of Aircraft Emissions on Atmospheric Ozone

Most present-day jet aircraft cruise at an altitude range of 9 to 13 km that contains portions of the upper troposphere (UT) and the lower stratosphere (LS). Because these two regions are characterized by different dynamics and photochemistry, we have to make a distinction between exhaust gases released in the UT and those emitted in the LS. This is complicated because of the highly variable character of the tropopause. [Gettelman 99] estimated that stratospheric releases account for 20% to 40% of the total emissions.

[2] NO_x designates as well NO as well as NO_2

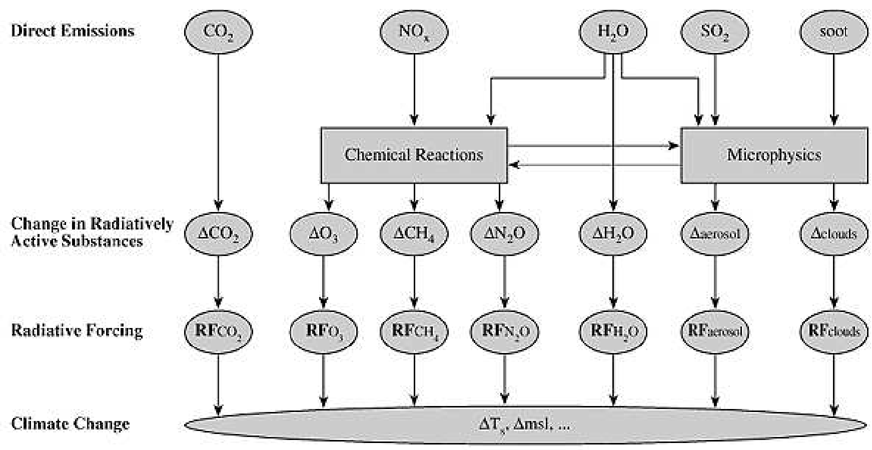

Figure 3: Schematic of possible mechanism whereby aircraft emissions impact climate (taken from [IPCC 99])

Approximately 80 % of atmospheric ozone resides in the stratosphere. Both in the troposphere and in the stratosphere ozone is mainly produced by in situ photochemistry. In both regions photochemistry also destroys part of the ozone and there is a downward flux of about 7% to 20% of the total stratospheric ozone mass from the stratosphere to the troposphere [Wauben 97]. Another sink for ozone in the lower troposphere is surface deposition.

To fully understand the impact of NO_x emissions on atmospheric ozone we have to look at the production of ozone in the region where commercial aircraft fly, which is done mainly by the oxidation of CO:

$$\begin{aligned} &OH + CO \rightarrow H + CO_2 && (1)\\ &H + O_2 + M \rightarrow HO_2 + M && (2)\\ &HO_2 + NO \rightarrow NO_2 + OH && (3)\\ &NO_2 + \text{sunlight} \rightarrow NO + O && (4)\\ &O + O_2 + M \rightarrow O_3 + M && (5)\end{aligned}$$

$$\text{Net}:\ CO + 2\ O_2 \rightarrow CO_2 + O_3$$

(where M designates a gaseous third body such as N_2 or O_2). We thus see that NO_x acts as a catalyst of the reaction and an increasing of NO_x concentration at cruising altitude will result in an increase in the rate of ozone production.

Furthermore it can be shown that NO_x and HO_x[3] are linked by a number of important reactions and the concentration of each depends on the concentration of the other(see [IPCC 99] p. 37). This implies that an increase in NO_x concentration induces also an increase in the destruction rate of ozone, because this is made mainly via the process:

$$O_3 + HO_2 \rightarrow OH + 2\ O_2.$$

Some studies (namely the NASA-sponsored SUCCESS campaign) on this subject have shown that in the UT and the lowermost stratosphere (below approximately 16 km), where all subsonic

[3] HO_x represents OH and HO_2

commercial aircraft fly, an increase in the concentration of NO_x will lead to an increase of ozone concentration.

As we have seen previously aircraft engines also release aerosols into the atmosphere. Of these, aircraft sulfate and water-ice particles will remove the ozone precursors HO_x and NO_x in the UT, and liberate ClO_x in the LS, which tend to destroy ozone. Thus aerosol particles have an opposite effect on ozone concentrations compared to NO_x.

Thus Aircraft emissions have different counteracting effects on atmospheric ozone and it is necessary to use chemistry and transportation models of the atmosphere, as well as in situ observations to define the overall impact of current aviation on ozone.

There has been no experimental evidence for a large geographical impact of aircraft on chemistry anywhere inside the troposphere, but the very good understanding of UT and LS processes involved in creation and depletion of ozone leads to the conclusion that ozone increases from aircraft NO_x, are on the order of 8 ppb, equivalent to a 6 % of the total ozone concentration.

1.1.2 Impacts of Aircraft Emissions on Methane

Reaction (3) shows that an increased NO_x concentration leads to an increase in the OH radical concentration in the atmosphere. This leads then to a decrease in CO concentration through reactions (1) and (2). Due to the longer lifetime of CO[4], these regions with lower CO concentrations spread out from airtraffic corridors toward the Equator. In the tropical and subtropical regions the where CH_4 is oxidized the lowering in CO levels and the induced augmentation of OH levels, leads to a slight decrease in CH_4 levels, so that the total flux through reaction (6) remains in balance with CH_4 emissions:

$$OH + CH_4 \rightarrow CH_3 + H_2O \qquad (6)$$

This results in a steady-state in which concentrations of CH_4 are slightly reduced. This readjustment of methane concentrations leads to a further increase in OH levels, and thus CH_4 concentrations build up more slowly over 10 to 15 years[5]. [IPCC 99] suggested that lifetime of methane is reduced by 2 %, but [Isaksen 04] showed that this figure is only about 1 %.

1.2 Aircraft Aerosol's Impact on Cloudiness

Aircraft flying around the tropopause have a direct and an indirect impact on global cloudiness. The direct impact is due to contrails[6], which represent artificially induced cirrus clouds that form under certain meteorological conditions in the plume of airliners. Additionally, aerosols emitted at high altitudes may serve as condensation nuclei for a general increase in cirrus clouds.

1.2.1 Contrail Formation

In the plume of an aircraft there is an increase in relative humidity (RH), that occurs as a result of warm moist exhaust gases mixing with colder and less humid ambient air. The RH must reach 100% during this process for contrails to appear. For climatological purposes only persistent contrails that have a lifetime of a few hours up to a few days are relevant.

Figure 4 shows us observations from several studies. The first one was done while contrails were clearly visible. In the second case they were on the limit of formation or disappearance, and in the third case no contrails at all were observed. Liquid and ice saturation are shown by the solid and dashed line respectively, as a function of H_2O partial vapor versus temperature.

[4] they may approach 2 months
[5] for more details about these reactions see [IPCC 01]
[6] this is a short form used for condensation trails

The thin line connected to each symbol represents the mixing line of plume states between ambient and engine exit conditions, for different types of aircrafts. The mixing process in the expanding exhaust plume is close to isobaric, that is why the mixing lines follow a linear rule in this graph, and the slope of each line is given by ([IPCC 99] pp.77):

$$\mathrm{EI(H_2O)c_pp[0.622Q}(1-\eta)]^{-1}, \tag{1}$$

where $\mathrm{EI(H_2O)}$ is the emission index of water vapor[7], c_p it the specific heat capacity of air, the ambient pressure is given by p, 0.622 represents the ratio of molar masses of water and air, and the effective specific combustion heat is given by $Q(1-\eta)$[8].

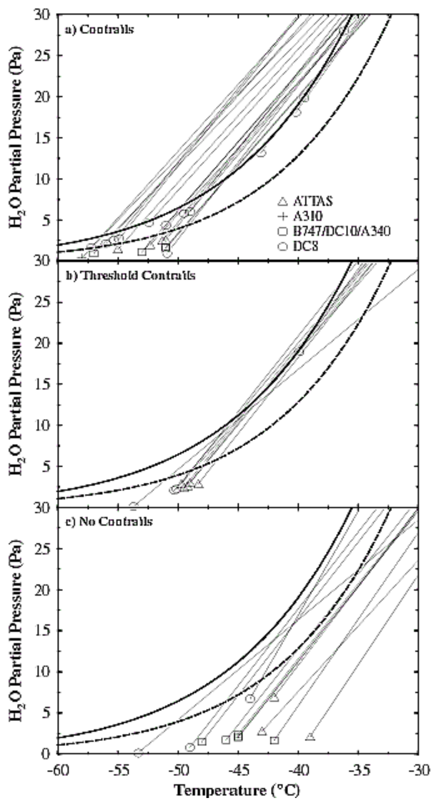

Figure 4: Water vapor partial pressure and temperature measurements from various contrail studies (taken from [IPCC 99])

From these graphs we can see that contrails only from if the mixing line crosses or at least touches the liquid water saturation curve. Furthermore contrails are persistent when mixing-line endpoints fall between the liquid and the ice-saturation curves in figure 4. in this case the ambient atmosphere is supersaturated with respect to ice and ice-particle formed in the exhaust plume of aircraft engines, can grow by accumulation of supersaturated water from the surrounding air.

[7] The mass of material or number of particles emitted per burnt mass of fuel

[8] η is the overall efficiency of propulsion of an aircraft and defines the fraction of fuel combustion heat that is used to propel the aircraft. Only the fraction $(1-\eta)$ of the combustion heat Q leaves the engine with the exhaust gases

Young contrails are easy to detect, because of their characteristic line shape and because they are formed of relatively small particles[9]. They spread as a result of turbulence caused by aircraft vortices and become wide and thick enough to induce a radiative disturbance and can thus be detected by satellites[10] due to different radiative properties from natural cirrus. However it is very hard to detect aging contrails because they evolve into cirrus clouds, and lose their line shaped appearance.

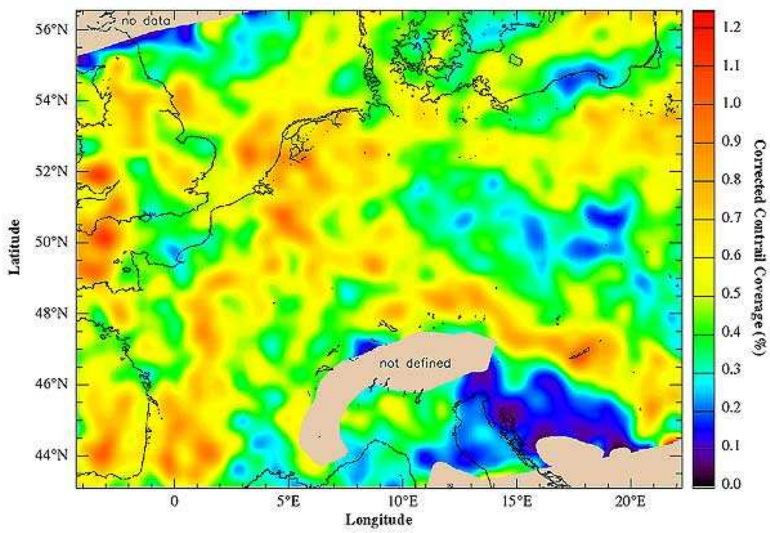

Figure 5: Annual mean contrail coverage at noon over mid-Europe in 1996, as derived from AVHRR data from NOAA-14 satellite (taken from [IPCC 99])

1.2.2 Increased Cirrus Clouds Coverage due to Aircraft

Cirrus clouds are high-level clouds forming at the edge of the troposphere and they are mainly composed of ice crystals. In the tropics cirrus clouds form due to deep convection whereas in the middle latitudes they are mainly induced in supersaturated regions of the upper troposphere. Their formation is strongly dependent on the existence of small particles which are acting as condensation nuclei.

Due to their cruise altitudes in the vicinity of the troposphere subsonic aircraft are thought to have an impact on cirrus cloud coverage in the main traffic corridors. First of all cirrus cloud coverage is induced by the presence of persistent contrails. Furthermore the release of particles by aircraft might induce changes in the properties of cloud condensation nuclei, but this effect is still quite uncertain.

[Zerefos 03] have compared cirrus cloud cover using satellite data of adjacent regions with high and low traffic (see figure 6). The comparison was done for adjacent regions to limit errors due to satellite calibrations as well as to minimize differences due to illumination geometry. In addition care has been taken to eliminate effect of natural phenomena from observational data.

The results show increasing trends in cirrus cloud coverage between 1984 and 1998 over high air traffic corridors of North America, North Atlantic and Europe. Only the summer time over

[9]For the same ice water content, contrails with small particles are more effective in radiative forcing than contrails with larger particles

[10]e.g. the Advanced Very High Resolution Radiometer (AVHRR) on board NOAA polar-orbiting satellites

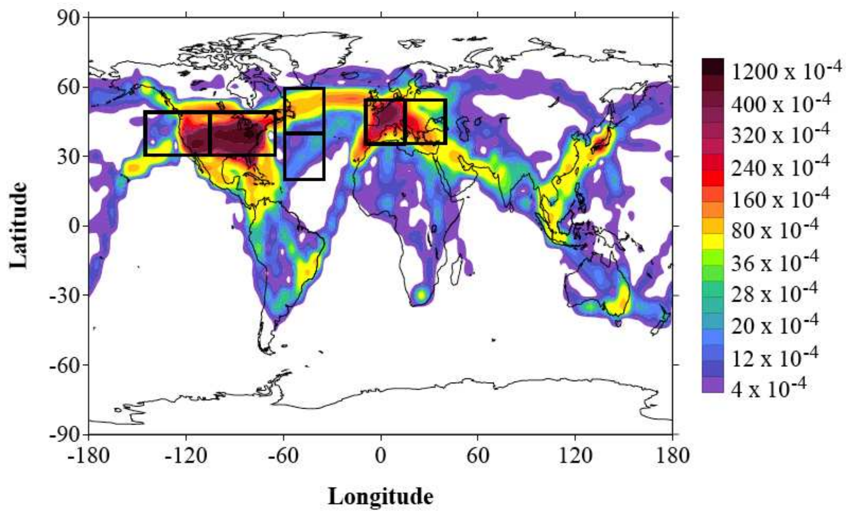

Figure 6: Total fuel consumption from aviation (in Tg of fuel) at 10-111 km height in wintertime. Rectangles correspond to regions with high and low air traffic in which cirrus cloud coverage averages have been studied (taken from [Zerefos 03])

the North Atlantic and the winter time over North America are statistically significant. Over the adjacent low air traffic areas, the calculated trends are mostly negative and statistically insignificant. This is in concordance with a general negative trend in cirrus cloud coverage[11]. The result of their work is shown in table 1.

Table 1: Seasonal and annual trends in cirrus cloud coverage from ISCCP satellite cirrus cloud date set (1984–1998) for regions categorized as having high and low air traffic for 1992 aircraft operations. Values in brackets refer to statistical significance of each trend. Dashes in brackets indicate a confidence level less then 95%

Trend(%/decade)	Winter (DJFM)		Summer (JJAS)		Annual	
	HATR	LATR	HATR	LATR	HATR	LATR
North America	+2.1 (95%)	+0.9 (–)	+0.5 (–)	−1.4 (95%)	+1.3 (–)	−0.2 (–)
North Atlantic	−0.4 (–)	−0.7 (–)	+2.6 (99.5 %)	+1.2 (–)	+1.2 (95%)	+0.3 (–)
Europe	0.0 (–)	−1.3 (–)	+1.3 (–)	−0.2 (–)	+0.3 (–)	−0.8 (–)

1.2.3 Soot, Sulphate Particle and Chemi-ions

Today the conversion of fuel sulphur to sulphuric acid is thought to be of the order of 1 to 5 %, and is thus lower than the maximal figure of 20% given in [IPCC 99]. There exist two ways for water vapor to freeze:

- During homogenous freezing ice crystals are formed from pure water vapor that was cooled to temperatures several tens of degrees below the freezing point of water, i.e. at large supersaturation;

[11] This trend is due to the global warming of the climate

- Heterogeneous freezing occurs when other particles, which are present, cause the ice crystal to be formed already at temperatures closer to the freezing point.

Aircraft emit positive and negative chemi-ions[12] with masses up to 8500 amu[13] that promote growth and coagulation of particles. (see [Kiendler 02]).

[Lohmann 02] concluded that aircraft emissions of sulphate aerosols are not likely to be important for cirrus formation, but that soot emissions could be important if the soot particles nucleate more efficiently than by homogenous freezing. Combuster measurements have shown that exhaust soot contains a significant amount of organic material, which enhances its hygroscopicity. [Vancassel 04] have shown that ions may imply that 80% of the soot particles become electrically charged and thus hygroscopic. Soot may therefore act as condensation nuclei even if fuel void of sulfur is used.

1.3 Radiative Imbalances due to Aviation

Radiative forcing may be defined in several ways, but for this thesis the IPCC definition will be assumed. The main power source for earth's climate is the sun and our planet intercepts 340 Wm^{-2} of solar radiation over its surface, on average. About 30% of this radiation is reflected by the top of the atmosphere back to space. The rest penetrates the atmosphere to heat the planet. Globally there must be a radiative balance between this incoming short-wave radiation and the outgoing long-wave radiation at the top of the atmosphere. When greenhouse gases are altered by anthropogenic sources, this results in a radiative imbalance. The climate system adjusts certain factors — primarily the temperature and clouds of the the lower atmosphere — to restore the initial radiative balance. IPCC defines the radiative forcing (RF) to be the imbalance (expressed in Wm^{-2}) at the tropopause before such adjustment of the troposphere on a global annual mean. Thus by this definition the RF of the pre-industrial atmosphere is zero.

Figure 7 shows us the the mean radiative forcing from all perturbations due to air-traffic in 1992, based on the the understanding of the different processes in 1999, as well as an updated view of these perturbations, with the actual understanding. We are going to derive this updated view of this diagram in the following sections.

1.3.1 Radiative Forcing by Changes in greenhouse Gases due to Aviation

Due to the very long residence time of CO_2 in the atmosphere (of the order of many decades) aircraft CO_2 becomes very well mixed with that of other anthropogenic sources. The forcing due to aircraft emissions of carbon dioxide is directly proportional to to the amount of fuel burned. The radiative forcing for aviation CO_2 in 1992 was estimated by IPCC to be +0.018 Wm^{-2} with a likely range of ±30 % (see [WMO 99]).

Another long lived greenhouse gas is methane (a lifetime of about 9 years). As we have already highlighted subsonic aircraft tend to decrease the lifetime of CH_4 by ejection of NO_x. This instantaneous change of about −1.3 % in 1992 needs to be further increased by a factor of about 1.4 to include the feedback of CH_4 concentrations on lifetime (see [Prather 94]). This led [IPCC 99] to the conclusion that radiative imbalance on methane concntrations was about $-0.014Wm^{-2}$. As we have seen before these figures have been adjusted since then and [Isaksen 04] suggests an imbalance of $-0.008Wm^{-2}$ for CH_4.

On the other hand ozone is a very short-lived greenhouse gas. As we have seen previously, its production is increased by the emission of NO_x in the atmosphere. Modeling suggests that

[12] molecules that have taken up or released up to a few electron charges

[13] atomic mass units

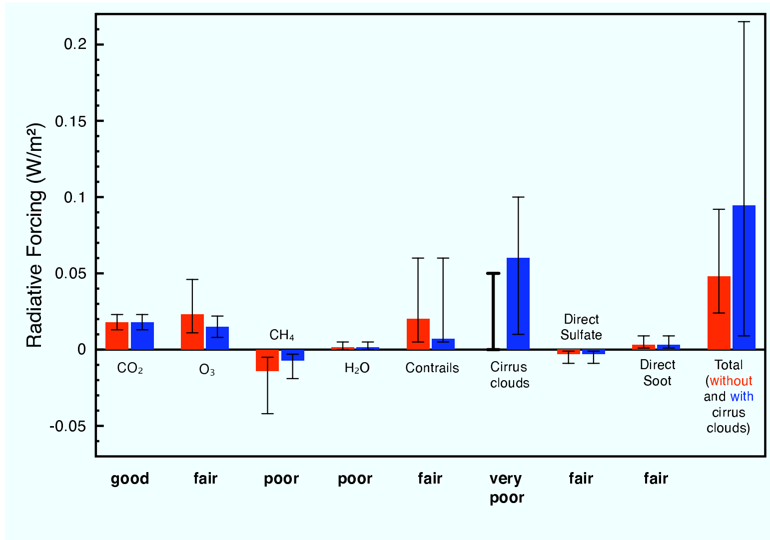

Figure 7: Radiative forcing from air traffic in 1992 as estimated by [IPCC 99] (red bars) and revised estimates for the 1992 fleet based on recent research results (blue bars) (TRADEOFF project). (adapted from [Schumann 03])

current emissions are responsible for an enhancement of 2 to 5 ppbv in the middle troposphere at northern mid-latitudes. Furthermore for methane as well as for ozone we may assume that the impact due to aviation may be scaled is proportionally to fuel emissions.

With this assumption the radiative forcing due to aircraft induced ozone enhancement was found to be +0.023 Wm^{-2} for NASA-1992*, a detailed 3-D pattern of NO_x emissions. However the uncertainty on this value is of factor of 3, and this is due mainly to the uncertainties in modeling the interaction between NO_x and O_3. [Isaksen 04] suggest that this figure may slightly lower, which is probably due to a better resolution of the models available today.

During the combustion of kerosene water vapor is produced. This also has a very short residence time in the atmosphere controlled by the hydrological cycle. As subsonic aircrafts fly in the troposphere most of the time, there is no accumulation of H_2O gases due to precipitation. This is also true for the part released in the LS, because flight paths are close to the tropopause, the released water vapor is rapidly returned to the troposphere (see [Holton 95]).

Even though the radiative forcing due to water vapor from aviation is only known with a big uncertainty (a factor of three) its absolute number in 1992 was sufficiently small (+0.0015 Wm^{-2}), that this presents a minor uncertainty for the overall forcing of aviation.

1.3.2 Radiative Forcing due to aircraft-induced Aerosols

This radiative forcing is due both to a direct and an indirect effect. The direct effect is due to the scattering and absorption of solar long-wave radiation by aerosols, whereas the indirect effect is due to cloud formation. Aerosol particles act as cloud condensation nuclei and modify the physical and radiative properties of clouds. Furthermore under certain meteorological conditions high flying aircraft produce contrails which perturb incoming solar radiation as well as outgoing thermal radiation.

One of the direct radiative forcing effects is due to sulfate aerosols which have a negative radiative forcing. In fact as a result of the size of aerosol particles, the direct radiative forcing of sulfate in long-wave radiation is likely to be negligible. On the other hand sulfate aerosols scatter a fraction of incident solar radiation, and thus contribute to a negative radiative imbalance. (see [Myhre 98]). The global mean direct radiative forcing due to sulfate aerosols is estimated to have a mean value of $-0.003\mathrm{Wm}^{-2}$ with a likely range of -0.001 to $-0.009\mathrm{Wm}^{-2}$.

Airliners also release black carbon aerosols in the atmosphere, also described as soot. These primarily absorb incident solar radiation which leads to positive radiative forcing if they are located in the troposphere. If soot is released in the stratosphere in contributes to a negative solar radiative forcing. Using the scenario NASA-1992, [IPCC 99] estimates forcing due to black carbon aerosols to be +0.003 (+0.001 to +0.006) $\mathrm{Wm}^{-2}$and it is assumed to be linearly scaled to fuel use.

1.3.3 Effects of Contrails and induced Cirrus Cloud Coverage

As can be seen on figure 7 [IPCC 99] only gives a best estimate for contrails but only a likely range for radiative forcing for induced cirrus cloud coverage by aviation.

The radiative impact of contrails depends on their fraction of sky area covered as well as their optical depth, which is controlled mainly by the radii of the droplets forming the contrail. [IPCC 99] adopted a best estimate value of +0.02 Wm^{-2} for radiative imbalance due to the global coverage of contrails, which is taken from [Minnis 99]. The likely range is between +0.005 and +0.06 Wm^{-2}. Presently this radiative forcing is thought to be a factor of 3 to 5 smaller. [Ponater 02] have developed a contrail parametrization model for global circulation models and they have found that contrails are optically thinner than estimated by [Minnis 99]. Moreover [Minnis 99] adopted for their radiative calculations a pressure altitude et 200 hPa, where radiative impact is largest, but which is unrealistic. [Marquart 03] gave a new estimate of the radiative impact of line shaped contrails which amounts to 0.0035 Wm^{-2} in 1992. Furthermore [Marquart 03] estimated that there was a an average daily contrail cover of 0.375 Wm^{-2} by contrails over Central Europe.

As we have seen in section 1.2.2 there is a strong correlation between aircraft densities and an increase in cirrus cloud coverage. This increase has been estimated by [Stordal 05] to be of the order of 0.25 % per year. Multiplying this mean estimate of change in cirrus with a mid range value of 0.12 Wm^{-2} per 1% cloud cover (see [Myhre 01]), they arrive to a mean global forcing of 0.03 (0.01 to 0.08) Wm^{-2}. This is in the upper region of the estimate made by [IPCC 99]

[Travis 02] have claimed that the difference between minimum and maximum temperature increased by 1 degree across the United States in the three days after the September 11 in 2001 when air traffic was stopped. If this was true, it would indicate that the effects of aviation on clouds are higher than currently estimated. But the statistical evidence of this effect is weak.

1.3.4 Total Radiative Impact of Aviation

[Sausen 05] have estimated that the best estimate of radiative forcing due to aviation in the year 2000 was of 0.048 Wm^{-2}. Since the 1992 base year of the [IPCC 99] results, emissions of CO_2 have risen but the radiative forcing for contrails is now estimated to be lower and thus this total radiative forcing is still fairly close to the figure reported by [IPCC 99].

Finally figure 7 shows an updated version of the radiative forcing by global aviation for the year 2000 (based on EU-project TRADEOFF). It should be noted that the total forcing now includes the cirrus clouds. The authors of the TRADEOFF-project estimate that the level of scientific understanding for each forcing has not changed significantly since 1999.

1.4 Integration over Time and Space

Due to the different resident times of green house gases perturbed by aviation in the atmosphere, there is a huge difference to their relative effect. Effectively, when assuming a decrease in air traffic, the forcing due to changes in cloud cover, and ozone is diminishing quickly within a few weeks. However for carbon dioxide there is an accumulation effect in the atmosphere, and thus changes take longer to have effect.

That's why IPCC proposed for long lived well mixed greenhouse gases (CO_2, CH_4, N_2O and hydrofluorocarbons) to use a global warming potential (GWP)[14] relative to CO_2 to compare their effects on climate change relative to carbon dioxide. [IPCC 99] concluded however that GWP cannot easily be applied to aviation, as all pulses for short lived green house gases and aerosols are different depending on location and altitude, but there may be other approaches such as the Global Temperature Potential proposed by [Shine 03].

In order to integrate aviation effectively into climate policy instruments such as the European Emissions Trading Scheme, some kind of index that permits a comparison between all impacts of aviation is needed. If only CO_2 would be included, this could lead to an important increase of NO_x and contrails.

[IPCC 99] proposed to use a radiative forcing index (RFI), which is defined as the ratio of total radiative forcing compared to that form CO_2 only, applied to future scenarios, to compare the total effect of other gases with CO_2, integrated over time. However this idea depends strongly on the chosen scenario and as we will show in section 5.1.2 radiative forcing of ozone is not linearly correlated to temperature change, when ozone is emitted at different altitudes. Moreover this index does not take into account the very strong geographical inhomogeneity of the radiative forcing of short-lived impacts (e.g. radiative forcing due to contrails in figure 8).

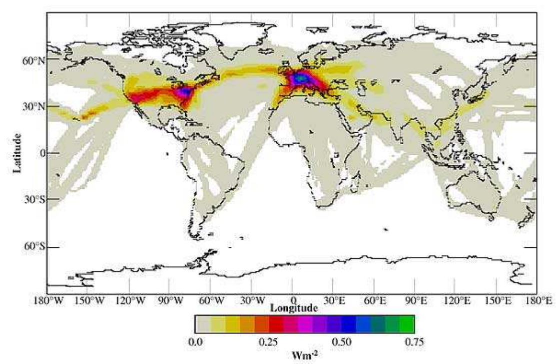

Figure 8: Global distribution of net instantaneous radiative forcing at the top of atmosphere in daily and annual average for 1992 climatic conditions and fleet. (from [IPCC 99]).

We see that the the simple choice about how to integrate over time and space, although it is a value judgement, may make much more difference to such indices and hence to the relative effect of different policies, than many of the scientific uncertainties. This is why there needs further research on how to integrate climate impacts due to aviation over space and time

[14]The global warming potential is defined by: $\mathrm{GWP} = \frac{\int_0^{th} a_x \cdot [x(t)]dt}{\int_0^{th} a_r \cdot [r(t)]dt}$, where th is the time horizon over which the calculation is considered (standard horizons for IPCC have been 20, 100 and 500 years) ; a_x is the radiative efficiency due to a unit increase in atmospheric abundance of the substance and $[x(t)]$ is the time-dependent decay in abundance of the substance following an instantaneous release of it at time $t = 0$. The denominator contains the corresponding quantities for the reference gas (i.e. CO_2).

CHAPTER II
FUTURE SCENARIOS

Between 1990 and 2005, traffic grew from 707,585 flights to 1,386,085 flights per month over Europe. This represents an increase of 96% in 15 years, and an average annual growth of 5%, consistent with the predicted growth of 3 to 5% given by [IPCC 99] . However in 2005, traffic reached unprecedented levels with a rise of 6.9% in 2004.

This shows that the aircraft sector is still in full expansion, despite the terrorists attacks in 2001 and the threat for epidemic diseases like SARS. This trend is not likely to stop before 2050 [IPCC 99], and so it is important to have scenarios that predict the future rise of global air transport, as well as the changes in emissions that are likely to occur.

This section explains the impact of different technologies on the emissions. Next we will analyze the effect of more efficient air transport operations and how they can be achieved.

As the AERO2k data gives emission for 2002 and 2025 (see chapter 3), so we will focus on the near future, and we will omit details about a hypothetical supersonic fleet that was postulted by [IPCC 99] to enter service after 2015, but which is not included in AERO2k.

2.1 Impact of Aircraft Technology on Emissions

The main factors that influence aircraft designs now and in the future are:

- Passenger safety must be assured for all phases of the flight.
- Volume and weight limitations are more severe than for ground-based means of transport.
- Changes aimed at improving one aspect (e.g. pollutant, safety, noise) may have undesirable affect on other aspects (e.g. fuel efficiency, NO_x emissions).
- It takes of the order of decades before new developments enter in service for the whole fleet
- Aircraft have high development, purchasing and operating costs, and so it is important to assess the impact of technologies changes on cost and customer satisfaction.

All these considerations need to be born in mind when a new aircraft is developed. Figure 9 shows how [IPCC 99] imagines a subsonic plane in 2016. The main achievements to increase fuel efficiency are also listed in this figure and I'm going to discuss them briefly in this section.

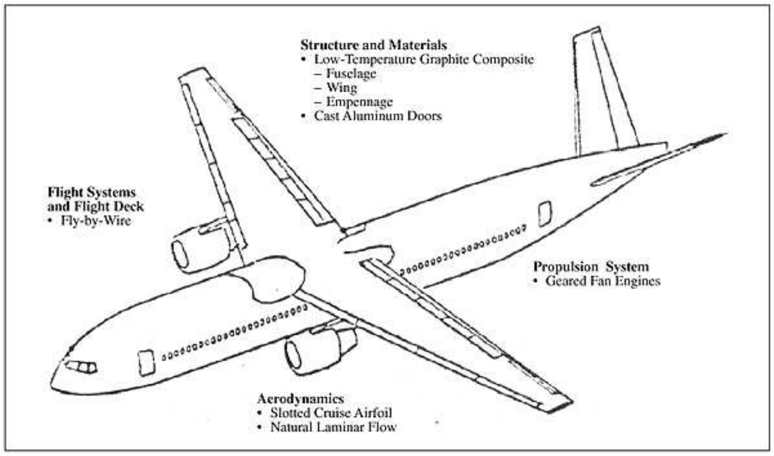

Figure 9: Subsonic airplane in 2016 (from [IPCC 99])

2.1.1 Airframe Performance

[IPCC 99] assumes that before 2020 it is not probable that there may be airframes which differ considerably from todays concepts (e.g. a blended-wing body[15]). So the main airframe achievements in the near future are going to be achieved by improving current concepts (e.g. Airbus A380), or even by adapting these concepts to derivatives of existing airplanes (e.g. Boeing B747-8).

These improvements can be laminar flow concepts, where drag is reduced by trying to get a laminar airflow for most part of the fuselage. This can be done by aerodynamic improvements or by laminar flow suction systems, which try to keep the flow laminar by sucking ambient air through porous skin. However these latest developments need further development and it is not likely that they will be ready to enter service before 2015.

The quest for further weight reduction is likely to go on and may be achieved by employing new materials that offer the same safety level as present materials(e.g. graphite composite, further use of aluminum[16]). Another weight reduction source is the reduction of passenger amenities. Whilst it is questionable that all fare-paying passengers would accept these reductions. In general the weight of amenities is likely to be further reduced. All these strategies for reducing weight combined could lead to a fuel efficiency improvement of 1%[17].

The integration of replacing current pneumatic systems by electric ones, as well as extending the use of fly-by-wire system could improve the fuel efficiency by 1 to 3%. On the other hand safety improvements could increase the operating empty weight.

All these measures together may lead to an augmentation of airframe performance by 10% between 1997 and 2015 and by 25% between 1997 and 2050. [IPCC 99]

[15]blended wing body: designates an alternative airframe design which incorporates design features from both a traditional tube and wing design into a hybrid flying wing configuration

[16]For some new materials (e.g.aluminum) it is important to consider also the energy to produce it. Thus these considerations need a full-life analysis

[17]The baseyear for all improvements is 1992

2.1.2 Key Points in reducing Fuel Use

As for aircraft development, safety and weight are key factors, it is unlikely that the hydrocarbon-powered gas turbine may be replaced by an alternative propulsion system in the next 50 years.

The overall efficiency[18] of an aircraft engine η_0 is given by the product of the thermal efficiency η_{therm} and the propulsion efficiency η_{p}. The thermal efficiency of a gas turbine is its ability to convert the chemical energy of the fuel into mechanical work (i.e., η_{therm} = power of the gas stream/ energy input rate). The propulsive efficiency is the ratio of the useful power to the increment in kinetic energy given to the flow passing through the engine. It is given in a good approximation by: $\eta_{\text{p}} = 2V/(V + V_j)$, where V is the flight velocity and V_j the jet velocity.

The main future gains in propulsive efficiency will be made by further increasing the bypass ratio of turbofan engines, which means enlarging the diameter of the propulsor. Bypass ratio above 10 requires the addition of a gearbox to the powertrain, which increases weight and complexity and so has to be balanced against total fuel efficiency of the plane. If the bypass ratio is over 15, duct has to be removed to contain weight and drag of the engine. These unducted fans of bypass ratios of 30 and more have been flown on test aircraft and gains of 25% of propulsive efficiency have been measured compared to modern engines.

There are more options to improve thermal efficiencies. Firstly, there are changes that can be applied to current approaches. These include further increases in the pressure ratio of compression and improved component efficiencies. To realize these goals a wide range of research and substantial investments are needed, but they may improve thermal efficiency by 10 to 20%.

Secondly, for future engines, there is potential for decreasing the weight of engines by 20 to 40%, by using alternative materials and improvements in aerodynamics inside the engine. This approach is particularly attractive because one unit of engine weight gain, saves between 1.5 and 4 units of aircraft empty weight, with an induced decrease in fuel burn. This is due to the fact that when engine weight is reduced supporting structure of the engines can also be reduced.

These improvements in thermal and propulsive efficiency may lead to an overall propulsion efficiency increase of 10% from 1997 to 2015 and of 20% from 1997 to 2050. Advances in both the airframe and the propulsion fuel-efficiency lead to a predicted increase of 20% from 1997 to 2015 and of 45% from 1997 to 2050.

2.1.3 Improvements in Emissions

Since engines with high bypass-ratio were introduced in the 1970s, there has been a drastic reduction in CO and hydrocarbon emission index, but NO_x emission index have stagnated (cf. chapter 3, table 4). The main problem is that reducing nitrogen oxides emissions has an adverse effect on other performance characteristic and so a tradeoff has to be found.

The only way to reduce NO_x emissions without having a theoretical effect on carbon dioxide emissions is to reduce fuel-rich zones and the residence time in the combustor, without compromising any of the other characteristic parameters. This can be partially achieved by low-emission combustor technology, that includes premixing of fuel and air to control combustion temperatures. But even with these technologies measurements have shown that there is still a tradeoff between CO_2 and NO_x, although at lower NO_x levels.

The changes applied so far are relatively minor, but have had a significant impact as present state-of-the-art combustors emit 20 to 40% less nitrogen oxides than older ones. The next step in the near future will be the introduction of staged combustors, where the high-power stage can be optimized for low NO_x emissions, and does not have to cope with low-power stability

[18] The overall efficiency is the mechanical power created by the thrust divided by the energy input rate of the fuel flow.

requirements[19] These combustors reach a reduction of approximately 30% of NO_x emissions, but have the disadvantage to be more complex than present combustors, and need more sophisticated control units. Thus they can not fitted to existing airframes without major changes.

Current research goals are to achieve NO_x emissions reduction of 50 % in the coming years, and there is also research on future engines with NO_x reductions up o 70% below the current levels by using more advanced staged combustors.

2.1.4 Impact of Fuels on Emissions

Within the narrow limits of aviation fuel control, variations have only very little impact on emissions, except for sulfur content. The actual value of sulfur content is 0.05% on average and is likely to stay at this level in the future, if there are no downward legislations.

All sulfur in the fuel is converted to sulfur oxides during combustion. For fuels with different sulfur contents[20] [**Schumann 96**] observed that the high sulfur contrail grew more quickly but also evaporated earlier than the low-sulfur contrail. The high-sulfur contrail also had a larger optical thickness and remained visible at slight higher temperature (0.2 to 0.4K). The particle measurements showed that the high-sulfur plume shows more particles with differences of about 25% for particles above 7nm and of 50% above 18 nm.

In general we can say that reducing sulfur content in aviation fuel, leads to a reduction in aerosols as well as soot particles, as well as a slight decrease in contrail coverage. However the sulfur is removed by hydro-processing. For this process hydrogen is needed and the most efficient way to produce it is by steam reforming of methane. This process creates carbon dioxide. A calculation shows that when aircraft would fly with sulfur free kerosene, there would be an increase of 0.1% of CO_2 attributable to aircraft.

2.2 Impact of Air Transport Operations on Emissions

In this section I'm going to explain how new system and procedures for Air Traffic Management (ATM) can reduce unnecessary emissions, produced by inefficient routing, cruising at less than optimum flight levels and airborne holdings. Non-ATM operational factors are addressed in the second subsection, which include optimization of aircraft utilization and speed, reductions in weight, limiting the use of auxiliary power as well as reducing taxiing.

2.2.1 Optimization of Air Traffic Management Systems

The key mission of ATM is to make efficient use of finite airspace and airport resources while guaranteeing a high level of safety. It is assumed that future changes will be based on new technologies and a creation of a more efficient and global ATM system.

In the existing worldwide structure planes have to fly along air corridors instead of flying on the most economic route (generally great-circle routes), which would also take wind, temperature, and other factors such as aircraft weight, charges and safety, into account. The present system is assumed to add about 9 to 10% to the flight track distance on average. This figures are much higher for short-haul flights.

EUROCONTROL supposes that such a "direct fight gate-to-gate" system could bring fuel savings of 7 to 8% in Europe. Though in the near future it is difficult to implement this direct flight strategy in the lower airspace, in dense populated areas as Europe and the United States

[19]These are mainly the prevention of a flameout during engine deceleration, and ignition at high altitudes and low temperatures, after an unscheduled shutdown.

[20]For this experiment a two-engined aircraft flew at an altitude of 9 km and burned a fuel with 0.016% sulfur content in the left engine and a fuel with 0.5% sulfur content in the right engine.

without compromising safety. Another scenario implemented by EUROCONTROL, is a free routing above 10, 200 m, and this could bring a benefit of 1 to 2 % in fuel-use.

This more efficient routing scenario has to be complemented by more precise weather information which has to be more accurate over a longer period. But also the current alphanumeric massages that are transmitted to flying planes can be changed into graphical information by the use of modern communication technology.

Another reason for excessive fuel burn can be flying below the optimal flight altitude due to saturation of the higher flight levels. One solution is to reduce the separation between flight levels which is possible due to more accurate altimeters for high altitudes. This Reduced Vertical Separation Minimum (RVSM[21]) is currently active in most parts of the world. More efficient routings and the aborting of flight routes will also lead to more vertical space available.

Finally it is important to improve and synchronize Terminal Maneuvering Area (TMA) operations in order to limit holding procedures and increase capacity. This can be achieved by the use of high-data-rate surveillance radar, as well as improved guidance system for approaching planes in instrument meteorological condition (IMC[22]), which both allow a more efficient flow for approaching airplanes on parallel and converging runways.

2.2.2 Operational Use and Emissions

Because of economic pressures the following points have already been optimized by airlines. The load factor[23] has the greatest impact on fuel consumption. Several statistics show that the load factor has increased in the past decade on an average of 0.4%, but it is unclear whether the load factor can continue to grow without consequences for passenger service.

The introduction of flight management systems has permitted calculation of the most economic speed on a real-time basis, taking into consideration actual weather information and state of aircraft. Due to this it is unlikely that there will be further reductions in fuel use by speed optimization on future aircraft[24].

Also weight reductions are possible due to operational use of aircraft. It is possible to reduce tankering[25] and achieve in this way a gain of about 0.5% of total fuel use of the total fleet.

Ground-based emissions can also be potentially reduced. On the one hand we have the use of Auxiliary Power Units (APU[26]) which can be reduced by the use of ground-based equipment that delivers electrical energy and preconditioned air to the aircraft. These operations could lead to savings of about 95% in APU fuel consumption, still and all the amount of total fuel saved is relatively small as it is estimated that APUs use less than 1% of total fuel used by aircraft.

For taxiing, there are several solutions that have been discussed. The first one is an optimization of traffic flow by ATC in order to minimize waiting times with running engines on the

[21] RVSM reduces the vertical separation between flight level (FL) 290 and 410 from 2000 ft to 1000 ft and makes six additional FL available for operation. Flight Levels are surfaces of constant atmospheric pressure which are related to a specific pressure datum, 1013.2 hPa, and are separated by specific pressure intervals. Flight levels are expressed in three digits that represent hundreds of feet

[22] see chapter 3

[23] The load factor gives the percentage of seats filled

[24] This is only true under the assumption that there are no major change in the composition of the fleet. However if priorities may change to environmental aspects, it is possible that slower flying planes may be favored.

[25] Tankering is the term used for loading fuel used for subsequent flight segments. Tankering is performed mainly due to commercial reasons. For example, in cases where the cost of fuel consumed in carrying additional fuel is more than offset by the difference in the price of fuel at the departure point and a destination where fuel could be loaded

[26] APUs are engine-driven generators that are usually contained in the tail of an aircraft and provide the aircraft with necessary energy during the time when engines are not running. Part of this energy is used for air conditioning

ground. Furthermore the use of high-speed taxiways, towing of aircraft to runways or taxing with minimal engines running could further reduce fuel consumption while an aircraft is on the ground.

The further optimization of these factors is of the order of 2 to 6%.

There is also a tradeoff between noise exposure and emissions. As a rule of thumb it is assumed that for a new aircraft design to achieve a noise reduction of 3 decibel, fuel burn is increased by 5%. For older engines it is possible to retrofit noise abatement equipment ("hushkits"), which can lead, mainly due to weight increase, to an increase of up to 5% in fuel use. In addition noise restriction may cause flight paths, arrival paths and departure paths to be longer than the shortest routings and may result in an increase in fuel consumption.

2.2.3 Changes in flight Altitudes

We have seen in chapter 1 that the radiative forcing of induced cirrus cloud cover is on the order of magnitude of that of carbon dioxide. Currently aircraft are designed to fly as high as possible. Also aircraft operators try to get the fleet flying as high as possible to reduce fuel consumption. But current atmospheric models predict that reducing flight altitudes will strongly reduce contrail occurrence and will aslo reduce the formation of ozone from aircraft NO_xemissions. On the other hand this reduction in flight altitudes will lead to an increase in flight carbon dioxide emissions. For instance [**Williams 02**] showed that decreasing flight altitudes by 6000 feet would lead to a reduction of contrail radiative forcing by a factor of two. All other effects are an order of magnitude smaller, e.g. CO_2 emissions would increase only by about 6 %.

Due to the very long residence time of carbon dioxide in the atmosphere compared to contrails and ozone concentrations, the reduction of flight altitudes is not considered to be the best solution to the augmentation of CO_2emissions. Another solution to minimize the impact of cloud changes due to aviation is to fly higher, in the stratosphere. Due to the very dry in this region of the atmosphere, there are no supersaturated air masses and thus contrails are very short lived.

Moreover this would reduce fuel consumption due to the reduction of density of the air. Actual subsonic planes are uncapable of reaching such high altitudes due to structural reasons, and also due to the high concentration of ozone, which needs the installation of filters in the climatic system of the airplane. But even if newer plane were able to reach such altitudes studies need to determine their impact on climate change, because the physics and chemistry involved are different from those of the troposphere.

CHAPTER III
Aircraft Database

The United Nations Framework Convention On Climate Change (UNFCCC) has recently published [UNFCCC 05] a comparison between data from different aviation models made available to ICAO and the latest available inventory information from UNFCCC. The databases considered were:

- the AERO model developed by the Dutch Civil Aviation Authority in the period 1994 to 2000 and is an internationally accepted tool for the computation of aviation emissions;
- the AERO2k project that was supported through the European Commission Fifth Framework program, which developed a new four dimensional gridded database of global aircraft emissions of priority pollutants using improved methodologies and analytical tools;
- the SAGE project developed by the United States Federal Aviation Administration (FAA) and which is based on the best available data and methodologies, and undergoes periodic updates to maintain currency.

For this thesis we chose to use the AERO2k Global Aviation Emissions Inventories (referred to as AERO2k) because the data was easily available and the used method to derive the data was estimated to give accurate results.

AERO2k provides a database for emissions in 2002 and 2025. For civil[27] aviation the data consists of fuel-used, NO_x, H_2O, CO_2, CO, hydrocarbon and particulate emissions in each grid cell. Moreover the distance flown in each grid cell is indicated. The grid cells have have a horizontal extension of 1 °by 1°, and a vertical height of 500 feet.

This chapter gives an overview of the way the AERO2k data was determined we will give an overview of the scenario for 2025 that was used to get the corresponding database. Finally we will talk about the possible sources of errors as well as their estimated amplitudes.

3.1 Acquisition of Data

The AERO2k data includes only aircraft that fly under instrumental flight rules (IFR)[28], because for these flights data is obtainable as they have to file a flight plan. Aircraft flying under visual

[27] The AERO2k data also includes a database for military aviation, but we will limit our consideration to civil aviation.

[28] If an aircraft is operated under instrumental flight rules, pilots rely on information displayed on instrument or equipment displayed within the aircraft for navigation and attitude holding. They have to file a flight plan with air traffic control before departure.

flight rules (VFR)[29] are excluded as no data is available. These aircraft can be considered as general aviation and helicopters and are estimated to use approximately 2 % of total global aviation fuel [Eyers 04].

3.1.1 Flight Routes

The flight-routes are obtained from different sources, including flight plans and timetables. Moreover for North America and the ECAC[30] area air traffic control data was used. For those regions where no radar data was available great circle routing was supposed. These regions represent less than 30% of the movements of global aviation. As the flight data comes from various sources, flights may be duplicated and trajectories may be present in a source but not in the other (see figures 10 and 11 for an example with ETMS[31] and AMOC[32] sources). In this case an algorithm was developed for merging trajectories in order to cover the longest trajectory possible.

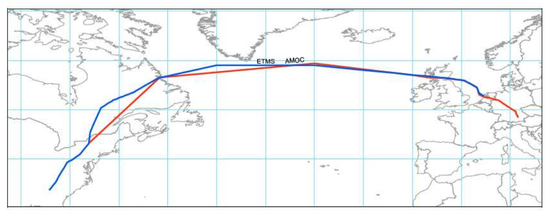

Figure 10: Same flight identified in ETMS and AMOC sources (from [Eyers 04])

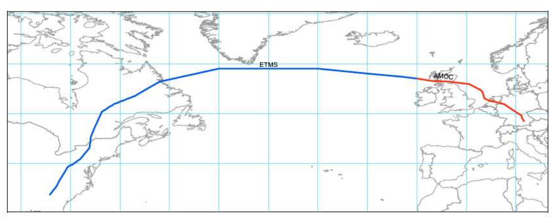

Figure 11: Same flight as in figure 10 after merging both sources (from [Eyers 04])

3.1.2 Aircraft Representation

After this flight database has been established it is necessary to know which plane equipped with which engines is used on a specific flight. In order to keep the modeling in manageable

[29] Aircraft flying under visual flight rules can only fly if visibility and ceiling permits a navigation via terrestrial navigation. VFR flights can navigate in lower airspace without flight plan.

[30] ECAC: European Civil Aviation Conference, including the 25 states of the European Community as well as Albania, Armenia, Azerbaijan, Bosnia and Herzegovina, Bulgaria, Croatia, Georgia, Iceland, Moldava, Monaco, Norway, Romania, Serbia and Montenegro, Switzerland, The former Yugoslav Republic of Macedonia, Turkey and Ukraine.

[31] Enhanced Traffic Management System, used by the Federal Aviation Administration (FAA) along with other systems to manage the flow of air traffic within the National Airspace System.

[32] Air traffic flow management MOdeling Capability, is used by Eurocontrol to develop and maintain the macroscopic air traffic management simulation capabilities.

proportions it was necessary to make simplifications regarding the global fleet of aircraft. Forty representative aircrafts, with their corresponding engines, were chosen so that, combined, they are representative of the entire fleet in terms of performance, fuel use and emission production.

The AERO2k database contains planes of four different aircraft types:

- Large jets: Jets having a capacity of over 100 seats. They are used to fly 76.38% of total distances of IFR flights in 2002.
- Regional Jets: Short-range aircraft powered by turbofan or turbojet engines, whose capacity does not exceed 100 seats. They covered 8.93% of the distance flown in 2002.
- Turboprops: aircraft that are powered by two or more turboprop engines. They flew 8.49% of total distances in 2002.
- Business Jets: Small planes with equipped with turbofan or turbojet engines and a capacity not exceeding about 20 seats. 6.20% of the distance in 2002 was covered by business jets.

The proportion of fuel used is roughly proportional to the percentage of distance travelled, and thus the large jet category was the primary focus and resulted in the largest number of representative types.

3.1.3 Emissions and Assumptions

Carbon dioxide and water vapor are in first approximation directly proportional to fuel use. A complete oxidation of a 1kg of Jet A-1[33] produces 3156 g of CO_2 and 1237g of water vapor [Eyers 04]. For a real combustion partially or unburned species (CO and hydrocarbons) have to be subtracted. Measurements show that the amount of hydrocarbons is less than 1% of the CO_2 and H_2O emissions and is therefore neglected. After the CO emissions have been determined, they are subtracted from the CO_2 emissions, taking into account the difference in molecular mass.

As carbon monoxide and hydrocarbon result from an incomplete combustion they are directly coupled with the combustion efficiency which can be determined indirectly from parameters in emission databanks of engines.

The production of thermal[34] nitrogen oxides in the combustor depends on the temperature and the residence time. However this data is not publicly available, and so an empirical relationship has been established between $EINO_x$ and fuel flow. In general the emissions predicted are in good agreement with measured emissions (see figure 12), although there seems to be an underestimation of about 12% on average. But this 12% deviation lies within the uncertainties.

It is important to note that the initial NO_x emitted from the engine jetpipe contains approximately 5 to 10% NO_2. Further conversion takes place, in the plume of the aircraft, and the final rate depends on properties of the plume, the speed and the altitude of the aircraft.

AERO2k is the first global emission database that also gives an approximation of soot and particle number emitted. The soot production is very complex and varies strongly with different engines, fuels and thrust settings. Furthermore the soot concentrations is not measured for the ICAO certification process, only the smoke number[35].

The soot concentration is determined in two steps. It is first determined for sea level static conditions out of the smoke number measurements of the ICAO database for every representative

[33] for definition see chapter 1 p. 6. The mean total formula of Jet A-1 is $C_{12}H_{23}$

[34] NO_x formed through high temperature oxidation of the diatomic nitrogen found in combustion air

[35] A dimensionless term quantifying smoke emissions. Smoke Number is calculated from the reflectance of a filter paper measured before and after the passage of a known volume of a smoke-bearing sample.

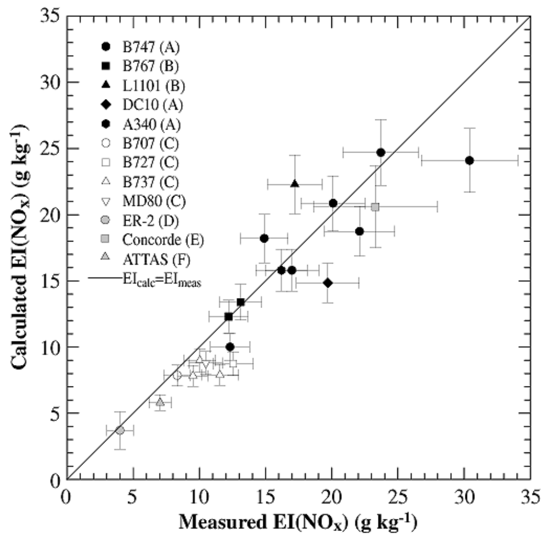

Figure 12: Comparison of measured values of EI(NO_x) with predicted values (from [IPCC 99])

engine. In a second step the actual emission index of soot depending on the altitude and speed of the aircraft is determined.

To determine the particulate number emitted it was assumed that a log-normal[36] distribution is a good representation of the real size of aircraft engine soot particles. A correlation of the mean diameter (μ) and the geometric standard deviation (σ) with engine parameters was developed from available data, and it was observed that the μ is growing with increasing combustor inlet temperature and pressure, whereas the standard deviation is not dependant on engine parameters but only on soot mass concentration, which was determined previously. Finally the particle number concentration was evaluated based on a model that uses the soot mass concentration and the particle size distribution.

3.2 Assumptions for 2025 Forecast

The gridded forecast for 2025 in AERO2k was calculated from the data of 2002. The capacity and traffic efficiency were evaluated and assuming improvements in fuel efficiency the total fuel use for 2025 was calculated. Increases in pressure ratio relative to more stringent levels relative to CAEP4[37] were assumed, and fuel efficiency increases were deduced.

3.2.1 Forecasting Fuel Use

In order to calculate fuel use in the forecast year, capacity[38] needs to be determined. The 2002 database yields a capacity of $4.787 \cdot 10^{12}$ available seat kilometers (ASK). The capacity forecast for 2025 was based on predicted traffic growth provided by Airbus and a load factor increase from 0.7 in 2002 to 0.74 in 2025. This yielded a total capacity of $1.243 \cdot 10^{13}$ ASK for the forecast

[36] A distribution is log-normal if the logarithm of the random variable is distributed in a gaussian way.

[37] CAPE: Committee on Aviation Environmental Protection, CAPE4 refers to stringencies on emissions during the take off and landing cycle (below 3000 feet) that have been in place since 1st January 2004

[38] Capacity is the product of the actual distance traveled between departure and arrival airports, frequency and the seating capacity of the individual aircraft.

year. Thus we see that in this scenario capacity is multiplied by 2.5956, compared to the base year 2002.

The fuel consumption is derived from capacity growth using the concept of "traffic efficiency"[39] introduced in [IPCC 99]. The fleet efficiency in the base year was evaluated to be 31.91 ASK/kg. In accordance with [IPCC 99] it was projected to increase by 1.3% per year until 2009, 1.0% pa from 2010 to 2020 and 0.5% pa thereafter. This approach considers improvements in all areas mentioned in chapter 2. A calculation shows that global fuel is multiplied by 2.0834.

3.2.2 Future Nitrogen Oxides Emissions

The information we have established so far gives the capacity and the fuel consumption for 2025, but it does not offer any information on age profile that is needed to evaluate NO_x emissions.

In order to do this a model was established to evaluate the addition and retirements of aircraft models from the present fleet until 2025. In this model the narrow-body aircraft would retire by age 27, and the wide-body by 35. After the planes have reached that age they are replaced by a new representative type, with essentially the same seat band. For those aircraft that are not being replaced during the forecast period, they are modeled so that they always comply with the emissions stringencies.

Table 2 gives the stringencies that are applied to this model, as well as the emission index of NO_x($EINO_x$) that would be achieved if the total fleet was only composed of planes with current stringencies in place. The dates are chosen for modeling convenience only and do not imply a commitment for CAEP to introduce them.

Year	2002	2004	2010	2012	2016	2020
Stringency relative to CAEP4 %	0	20	40	40	50	64
Raise in PR relative to base year %	0	0	5	10	15	20
$EINO_x$of a new fleet (g/kg fuel)	13.171	10.887	9.013	9.639	8.84	7.457

Table 2: Stringency and raise in pressure ratio (PR) relative to 2002 used in the model

As was explained the stringencies only apply to aircraft that are newly introduced in the fleet and thus the $EINO_x$ of the actual fleet is higher than the value given in the last line of table 2, because of the long time aircraft remain in service. The model shows that the $EINO_x$ for the effective fleet in 2025 is 10.12 g/kg fuel. For the prediction year emissions of NO_x by aircraft is projected to be multiplied by 1.6008.

3.2.3 Regional Growth Factors

The Airbus forecast data on which the AERO2k calculations are based, gives the growth of capacity between city pairs, and it is thus possible to specify the multiplication factor of capacity, fuel use and NO_x emitted within a region and between regions. This method does not account for possible new airports and all growth is supposed to occur along existing routes. This is a limiting assumption for the forecast. Even if in Europe and the United States the density of airports is already relatively high, it should not be excluded that new airports will be build in developing countries. Furthermore as explained in chapter 2, new technologies may also lead to more fuel-efficient routings. Tables of the multiplying factors can be found on pp. 55 and 56 in [Eyers 04].

[39] Traffic efficiency is defined as the quantity of ASK performed per kg of fuel used

3.3 Tests and Uncertainties of the Inventory

In order to get an evaluation of the uncertainties of the inventory we are going to compare it with previous ones and I'm going to discuss the key assumptions as well as their implications on the figures of fuel use and the emissions.

3.3.1 Comparison with other Inventroies

A first test of database is to compare it with previous inventories. Table 3 gives the total fuel use and different emissions and compares them to previous studies, that were used in [**IPCC 99**], whereas table 4 gives emission indexes.

	Aero2k	**NASA1999**	**NASA1992**	**ANCAT 1992**	**DLR 1992**
Fuel Used	156	128	113.85	114.2	112.24
NO_x	2.06	1.69	1.44	1.6	1.6
CO	0.507	0.685	1.29	n/a	n/a
HC	0.063	0.189	0.26	n/a	n/a
P M	0.0039	n/a	n/a	n/a	n/a

Table 3: Comparison of total fuel use (Tg) and emission(Tg) for the civil fleet of different inventories.(P M = Particulate Mass)

	Aero2k	**NASA1999**	**NASA1992**	**ANCAT 1992**	**DLR 1992**
$EINO_x$	13.2	13.2	12.6	14	14.2
EICO	3.25	5.4	11.3	n/a	n/a
EIHC	0.4	1.5	2.3	n/a	n/a
EI P M	0.025	n/a	n/a	n/a	n/a

Table 4: Comparison of emission indexes(g/kg) for civil aviation fleet of different inventories.(P M = Particulate Mass)

Annual growth rates between 1992 and 2002 were of the order of 5% and thus air traffic has been multiplied by a factor of approximately 1.5 since 1992. The increase in fuel use between AERO2k and the other inventories is consistent with fuel efficiency improvements the region of 1% per year during this period. This increases in combustion efficiency were achieved by increasing pressure ratio and other technology improvements as described in chapter 2. These improvements also induce a significant reduction in the emission indexes of CO and HC. However the effect of increasing the pressure ratio has offset any improvements in NO_x limitation technology and hence we observe that emission index of NO_x remains more or less constant. This assumptions seems plausible if more stringent limitations of NO_xemissions will be released in future. Perhaps these future regulations could not only apply to take off and landing cycles, as for the present regulations but also to cruise flight.

Thus we see that these calculated figures are in good agreement with previous assessments taking into account the technology improvements that have taken place since 1992. The particulate mass calculated cannot be compared with previous inventories and as it is based on a restricted number of measurements it should only be seen as a first estimate.

3.3.2 Key Background Assumptions and Uncertainties

During a flight the prevailing wind may alter the speed of the aircraft relative to the ground. This implies that effective flight times may be longer or shorter depending on the meteorological situation. Moreover pilots try to alter their flight routes altitudes and speeds in order to mitigate wind effects to some extent. The data that was obtained from radar data intrinsically incorporates the effect of winds because they have a direct effect on flight times. For the rest of the world still air was assumed. Comparison of some of the predicted data with actual flight figures shows that global fuel emissions are increased of approximately 1.5% by the effect of winds.

Due to congesting of airspace, aircraft often have to fly holding patterns before they are given permission to land. Due to the fact that the time resolution of the radar data is not high enough to detect holding patterns, AERO2k provides only very limited coverage of the effects of holding. British Airways has calculated that supplementary fuel use, due to holding, is to be 1.2%[40] to of total fuel consumption of the airline. However this figure is thought to be skewed due to the very high number of British Airways at London's Heathrow airport, known for long holding times. Thus the global increase in fuel burn due to holding, is expected to be much less than this figure.

As the flight movement database does not include take-off weight, it is not possible to account for fuel tankering in the inventory. [IPCC 99] estimates that tankering increases the total aircraft fuel consumption by 0.5%. It is important to note that tankering is much more prevalent on small aircraft flying short-range missions than on long-haul flights.

Deterioration of engines and the airframe leads to an increased fuel consumption. This is mainly due to deterioration of engines parts, that have to be worked harder to produce the required thrust. Also deterioration of airframe parts increase drag and thus fuel consumption, but this is assumed to have only a small impact on fuel burn because an aircraft will not have all of its engines in a highly deteriorated state and because airframe deterioration only builds up slowly over many years. It is thus assumed that addition fuel consumption of the actual fleet is 3% higher than that of a brand new fleet. As these effects are partly included in data used to validation of the inventory it is assumed that AERO2k data represents effect of deterioration adequately.

Table 5 gives a summary of the different uncertainties that have been explained. As for emissions uncertainty table 6 gives the maximal deviation between measured data and derived values.

Impact	Increase in total fuel use
Winds	$\approx +1.5\%$
Holding	$< +1.2\%$
Tankering	$< +0.5\%$
Deterioration	$< +3\%$ (partly included)
Total	$< +6.2\%$

Table 5: Uncertainties

Even though in the previous section we derived that AERO2k was in agreement with other studies, the [UNFCCC 05] intercomparison noted that the flight-path approach of AERO2K

[40] Assuming that fuel consumption is directly proportional to holding time, this would lead to a average holding time of two minutes, for a three hours flight. This seems very low. Due to the fact that planes are flying much slower during holding, and that pilots try to use as less fuel as possible, the holding time is probably not proportional to total fuel use.

Emission Index	**Maximal deviation**
CO and HC (EI > 5 g/kg)	15%
CO and HC (EI < 5 g/kg)	0.3g/kg
Soot mass	10%
NO_x	5%

Table 6: Maximal deviation from measured emissions

tended to produce lower estimates of emissions, compared to the simple measurements of fuel sold collected by UNFCCC. Thus it seems that the theory is not matching the reality, perhaps the processes considered are treated accurately, but other processes are missing from the analysis, leading to a systematic error. The total uncertainties in table 5 do not add up to anything like so much as the figures derived by UNFCCC (e.g. for Belgium the AERO2k database only gave 69 % of the fuel sold). Moreover it was also shown in [**UNFCCC 05**] that AERO2k gives the lowest fuel consumptions of the three databases compared (AERO,AERO2k and SAGE).

SECOND PART

MODELING AVIATION IMPACT

CHAPTER IV
One Dimensional Convective Model

Now that we have discussed the impacts of aviation on climate as well as the future scenarios, we will give an order of magnitude of the different impacts by using a simple one dimensional radiative convective model (1DRCM). This chapter gives an overview of the structure of the model and afterwards we are going to explain how this model has been modified to simulate the impact of aviation on climate change in Europe.

4.1 Description of the Model

The model used was developed by R.M. MacKay and M.A.K. Khalil and was originally designed to evaluate the impact of different greenhouse gases (CO_2,O_3,CH_4,NO_2 and CFC's) on global climate change. We are going to give a description of these parts of the model only that are relevant for further use. For more information about other parts as well as for performance and sensitivity experiments please refer to [MacKay 91].

4.1.1 Vertical Structure

The model contains 18 atmospheric layers and one ocean mixed layer. The atmospheric layers extend from the surface to an altitude of approximately 42 km. The levels are counted from the top and their thickness is calculated in function of the pressure (given in atm). The pressure thickness ($\mathrm{dp_i}$) of each layer is defined as:

$$\mathrm{d}p_i = 6(\sigma_i - \sigma_i^2)\mathrm{d}\sigma,$$

with: $\mathrm{d}\sigma = 1/18$, $\sigma_0 = 0$ and $\sigma_i = (2i-1)/36$, for $i \in [1,18]$. Furthermore the pressure average of each layer is given by:

$$pa_i = \sigma_i^2(3 - 2\sigma_i).$$

The pressure at the top (p_i) and the bottom (p_{i+1}) of each layer are calculated by starting at $p_1 = 0$ and adding the pressure thickness of each layer going down: $p_i = p_{i-1} + \mathrm{d}p_{i-1}$, for $i \in [1,18]$. Figure 13 gives us the layer structure of the model, that has just been described.

The height z of each layer is calculated, by assuming that the atmosphere is vertically in hydrostatic equilibrium ($\frac{\partial p}{\partial z} = -\rho g$, where ρ is the density of the air, and g is the gravity

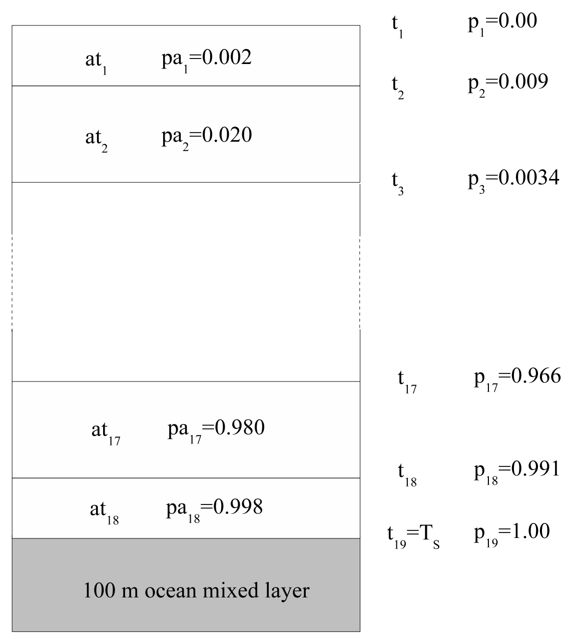

Figure 13: Schematic representation of the 1DRCM model of the Earth-atmosphere system. Pressures are given in atm.

acceleration). The pressure difference between the top and the bottom of layer i is given by: $\Delta p_i = p_{i-1} - p_i$, and the difference in height: $\Delta z_i = z_{i-1} - zi$. We thus have:

$$\frac{\Delta p_i}{\Delta z_i} = -\rho_i g. \tag{2}$$

As the atmosphere can be considered to be an ideal gas, the density is given by:

$$\rho_i = \frac{NM}{V} = \frac{pa_i\, M}{R\, at_i}, \tag{3}$$

where M is the mean molecular weight of the atmosphere, R the ideal gas constant and at_i the average temperature of layer i. Introducing (3) into (2), we get:

$$\Delta z_i = -\frac{\Delta p_i\, at_i\, R}{pa_i\, g\, M}.$$

hence we see that the height of each layer can be calculated knowing that $z_{19} = 0$ (surface), and knowing the vertical distribution of the temperature an the pressure. As the vertical distribution of the temperature is calculated at each time step the height of the levels is not fixed and has to be reevaluated at each time step.

4.1.2 The Plane Parallel Atmosphere

We will now give a description of the plane parallel atmosphere, that is used in the model. In this approximation the atmosphere is supposed to be horizontally homogeneous, and we thus neglect the sphericity of the globe. It can thus be represented by the z coordinate directed upwards ($z = 0$ at the surface).

We will now derive the upward $F^{\uparrow}(z)$ and downward flux $F^{\downarrow}(z)$ of radiation for a given altitude z of the atmosphere. In order to do this we need the general equation of isotropic radiative transfer.

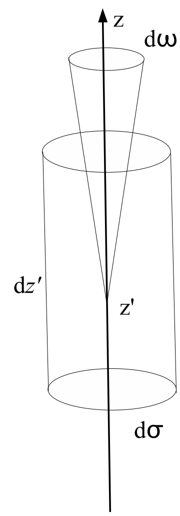

Figure 14: Cylindric volume at altitude z', of base $\mathrm{d}\sigma$, height $\mathrm{d}h$, whose axe is aligned with the vertical direction and the cone of solid angle $\mathrm{d}\omega$.

Let $L_\nu(z')$ be the monochromatic luminance of wave number ν at height z'. The equation of radiative transfer can be obtained by writing the energy balance in a small cylindric volume at height z', of base $\mathrm{d}\sigma$, height $\mathrm{d}z'$ and whose axe is aligned with the vertical direction (see figure 14).

The entering flux is given by:

$$\phi = L_\nu(z')\,\mathrm{d}\omega\,\mathrm{d}\sigma, \tag{4}$$

where $\mathrm{d}\omega$ is the solid angle of the cone originating at z' and directed along the vertical direction. The outing flux of the cylindric volume is given by:

$$\phi + \mathrm{d}\phi = \left(L_\nu(z') + \frac{\mathrm{dL}_\nu(\mathrm{z}')}{\mathrm{dz}'}\mathrm{d}s\right)\mathrm{d}\omega\,\mathrm{d}\sigma. \tag{5}$$

The flux lost by diffusion in this volume is given by:

$$\mathrm{d}\phi_1 = \sigma^{\mathrm{ext}}(z')\,\phi\,\mathrm{d}z' = \sigma^{\mathrm{ext}}(z')\,L_\nu(z')\,\mathrm{d}\omega\,\mathrm{d}\sigma\,\mathrm{d}z', \tag{6}$$

where $\sigma^{\mathrm{ext}}(z')$ is the coefficient of extinction at altitude z'. Finally the gained flux in the vertical direction is composed of diffused radiation coming from other directions than the vertical and by thermal emission in the volume element. In general this flux is written as:

$$\mathrm{d}\phi_2 = \sigma^{\mathrm{ext}}(z')\,J_\nu(z')\,\mathrm{d}\omega\,\mathrm{d}\sigma\,\mathrm{d}z', \tag{7}$$

where $J_\nu(z')$ is the source function at altitude z'. Conservation of energy implies that $\mathrm{d}\phi = \mathrm{d}\phi_2 - \mathrm{d}\phi_1$, and thus combining equations (4) to (7), this gives the general equation of isotropic radiative transfer:

$$\mathrm{dL}_\nu(\mathrm{z}') = -\sigma^{\mathrm{ext}}(\mathrm{z}')\,\mathrm{L}_\nu(\mathrm{z}')\,\mathrm{dz}' + \sigma^{\mathrm{ext}}(\mathrm{z}')\,\mathrm{J}_\nu(\mathrm{z}')\,\mathrm{dz}', \tag{8}$$

In the model the effect due to diffused radiation coming from other directions than the vertical is neglected, and thus the source function is approximated as :

$$J_\nu(z') = B_\nu(z'),$$

where $B_\nu(z')$ is the Planck function[41] for a perfect black body at the temperature of level z'.

Let us define the optical thickness (δ) between the altitude z and z' by:

$$\delta(z, z') = -\int_z^{z'} \sigma^{\text{ext}}(z'')\, \mathrm{d}z''. \tag{9}$$

In this model we approximate $\sigma^{\text{ext}}(z'') \approx 1.66\, k\, \rho$, where 1.66 is the diffusivity factor, ρ is the density of the air and k is the mass absorption coefficient. The monochromatic transmission function between layers z and z' is given by:

$$\begin{aligned} T_\nu(z, z') &= \exp[\delta(z, z')], \\ &= \exp\left[-\int_z^{z'} 1.66\, k\, \rho\, \mathrm{d}z''\right]. \end{aligned}$$

From (9) we deduce that:

$$\mathrm{dz}' = \frac{\mathrm{d}\delta}{-\sigma^{\text{ext}}(\mathrm{z}'')},$$

and the equation of radiative transfer (8) thus rewrites:

$$\mathrm{dL}_\nu(\delta) = \mathrm{L}_\nu(\mathrm{z}')\, \mathrm{d}\delta - \mathrm{B}_\nu(\mathrm{z}')\, \mathrm{d}\delta. \tag{10}$$

The downward luminosity at the level z is obtained by multiplying equation (10) by $T_\nu(z, z')$, and integrating from z to ∞. An integration by part then gives, noting that $T_\nu(z, z) = 1$:

$$L_\nu^{\downarrow}(z) = \lim_{z' \to \infty} L_\nu(z') T_\nu(z, z') - \int_z^{\infty} B_\nu(z')\, T_\nu(z, z')\, \mathrm{d}\delta.$$

In order to get a physical result we have to assume $\lim_{z' \to \infty} L_\nu(z')\, T_\nu(z, z') = 0$ (physically this means that the luminosity is zero when $z \to \infty$) . Noting that $\frac{\mathrm{dT}_\nu(\mathrm{z}, \mathrm{z}')}{\mathrm{dz}'} = T_\nu(z, z') \frac{\mathrm{d}\delta}{\mathrm{dz}'}$, we get:

$$L_\nu^{\downarrow}(z) = -\int_z^{\infty} B_\nu(z')\, \frac{\mathrm{dT}_\nu(\mathrm{z}, \mathrm{z}')}{\mathrm{dz}'}\, \mathrm{dz}'.$$

The monochromatic downward flux of radiation at level z is obtained by integrating the normal component of the luminosity, over all directions of the celestial hemisphere:

$$F_\nu^{\downarrow}(z) = \int_0^{2\pi} \int_0^{\pi/2} L_\nu^{\downarrow}(z)\, \cos(\theta)\, \sin(\theta)\, \mathrm{d}\theta\, \mathrm{d}\phi,$$

with θ is the azimuthal angle, and ϕ the zenithal angle. As we have assumed the luminance to be isotropic, this becomes:

$$F_\nu^{\downarrow}(z) = \pi L_\nu^{\downarrow}(z).$$

[41] The Planck function for temperature T and wave number ν is given by: $B_\nu(T) = \frac{2h\nu^3}{c^2 e^{h\nu/(kT)} - 1}$, where h is Planck's constant, c is the velocity of light and k is Boltzmann's constant.

To get the net downward flux at level z, we have to integrate over all wave numbers, which yields:

$$F^{\downarrow}(z) = -\int_0^{\infty} \mathrm{d}\nu \int_{\mathrm{z}}^{\infty} \pi\, \mathrm{B}_\nu(\mathrm{z}')\, \frac{\mathrm{dT}_\nu(\mathrm{z},\mathrm{z}')}{\mathrm{dz}'}\, \mathrm{dz}'. \tag{11}$$

To get the ascending luminosity at level z, we do a similar manipulation as previously with (10), but this time we integrate from 0 to z:

$$L_\nu^{\uparrow}(z) = L_\nu(0) T_\nu(z,0) - \int_0^z B_\nu(z')\, T_\nu(z,z')\, \mathrm{d}\delta.$$

Supposing that the surface is radiating as a black body, we have: $L_\nu(0) = -B_\nu(0)$. The net upward flux is thus given by:

$$F^{\uparrow}(z) = -\int_0^{\infty} \mathrm{d}\nu \left[\pi\, \mathrm{B}_\nu(0)\, \mathrm{T}_\nu(\mathrm{z},0) + \int_0^{\mathrm{z}} \pi\, \mathrm{B}_\nu(\mathrm{z}')\, \frac{\mathrm{dT}_\nu(\mathrm{z},\mathrm{z}')}{\mathrm{dz}'}\, \mathrm{dz}'\right]. \tag{12}$$

4.1.3 Expressions for infrared Fluxes

Equation (11) can be rewritten by using the monochromatic absorption function, given by: $A_\nu = 1 - T_\nu$:

$$F^{\downarrow}(z) = \int_0^{\infty} \mathrm{d}\nu \left\{\int_{\mathrm{z_t}}^{\infty} \pi\, \mathrm{B}_\nu(\mathrm{z}')\, \frac{\mathrm{dA}_\nu(\mathrm{z},\mathrm{z}')}{\mathrm{dz}'}\, \mathrm{dz}' + \int_{\mathrm{z}}^{\mathrm{z_t}} \pi\, \mathrm{B}_\nu(\mathrm{z}')\, \frac{\mathrm{dA}_\nu(\mathrm{z},\mathrm{z}')}{\mathrm{dz}'}\, \mathrm{dz}'\right\}, \tag{13}$$

where z_t is the altitude of the bottom of the top atmospheric layer which is assumed to be isothermal.

This implies that for the first integral in curled brackets in (13), $B_\nu(z') = B_\nu(z_t)$ is constant and can be factored out of the integral. The integral thus becomes trivial and gives:

$$\int_{z_t}^{\infty} \pi\, B_\nu(z')\, \frac{\mathrm{dA}_\nu(\mathrm{z},\mathrm{z}')}{\mathrm{dz}'}\, \mathrm{dz}' = \pi \mathrm{B}_\nu(\mathrm{z_t}) \left[\lim_{\mathrm{z}'\to\infty} \mathrm{A}_\nu(\mathrm{z},\mathrm{z}') - \mathrm{A}_\nu(\mathrm{z},\mathrm{z_t})\right].$$

As for the second integral of (13), an integration by parts yields:

$$\int_z^{z_t} \pi\, B_\nu(z')\, \frac{\mathrm{dA}_\nu(\mathrm{z},\mathrm{z}')}{\mathrm{dz}'}\, \mathrm{dz}' = \pi\, \mathrm{B}_\nu(\mathrm{z_t})\, \mathrm{A}_\nu(\mathrm{z},\mathrm{z_t}) + \int_{\mathrm{z_t}}^{\mathrm{z}} \pi\, \mathrm{A}_\nu(\mathrm{z},\mathrm{z}')\, \frac{\mathrm{dB}_\nu(\mathrm{z}')}{\mathrm{dz}'}\, \mathrm{dz}',$$

where we have noted that $A_\nu(z,z) = 0$ by definition.

Introducing these two results into (13) leads to:

$$F^{\downarrow}(z) = \int_0^{\infty} \mathrm{d}\nu \left\{\lim_{\mathrm{z}'\to\infty} \pi\, \mathrm{B}_\nu(\mathrm{z_t})\, \mathrm{A}_\nu(\mathrm{z},\mathrm{z}') + \int_{\mathrm{z_t}}^{\mathrm{z}} \mathrm{A}_\nu(\mathrm{z},\mathrm{z}')\, \frac{\mathrm{d}[\pi\, \mathrm{B}_\nu(\mathrm{z}')]}{\mathrm{dz}'}\, \mathrm{dz}'\right\}. \tag{14}$$

Let us define the broadband emissivity ϵ and the modified emissivity ϵ' to be:

$$\begin{aligned}
\epsilon(z,z') &= \int_0^{\infty} A_\nu(z,z')\, \frac{\pi B_\nu(z')}{\sigma T^4(z')}\, \mathrm{d}\nu, \\
\epsilon'(z,z') &= \int_0^{\infty} A_\nu(z,z')\, \frac{\mathrm{d}[\pi \mathrm{B}_\nu(\mathrm{z}')]}{\mathrm{d}[\sigma \mathrm{T}^4(\mathrm{z}')]}\, \mathrm{d}\nu,
\end{aligned}$$

With these definitions equation (14) rewrites, noting that $T(z_t) = \lim_{z'\to\infty} T(z')$, and $B_\nu = \lim_{z'\to\infty} B_\nu(z')$:

$$F^{\downarrow}(z) = \lim_{z'\to\infty} \sigma\, T^4(z_t)\, \epsilon(z,z') + \int_{z_t}^{z} \epsilon'(z,z')\, \frac{\mathrm{d}[\sigma\, \mathrm{T}^4(\mathrm{z}')]}{\mathrm{dz}'}\, \mathrm{dz}'. \tag{15}$$

In an analogous way as we have derived (14) we can derive the upward flux from (12):

$$F^{\uparrow}(z) = \int_0^{\infty} \mathrm{d}\nu \left[\pi\, \mathrm{B}_\nu(0) + \int_0^{\mathrm{z}} \mathrm{A}_\nu(\mathrm{z},\mathrm{z}')\, \frac{\mathrm{d}[\pi\, \mathrm{B}_\nu(\mathrm{z}')]}{\mathrm{d}\mathrm{z}'}\, \mathrm{d}\mathrm{z}' \right]. \tag{16}$$

Stefan's law says that $\int_0^\infty \pi\, B_\nu(0)\, \mathrm{d}\nu = \sigma \mathrm{T}(0)^4$ and we can thus rewrite this equation with the definition of the modified emissivity as:

$$F^{\uparrow}(z) = \sigma\, T^4(0) + \int_0^z \epsilon'(z,z')\, \frac{\mathrm{d}\sigma\, \mathrm{T}^4(\mathrm{z}')}{\mathrm{d}\mathrm{z}'}\, \mathrm{d}\mathrm{z}' \tag{17}$$

4.1.4 Calculation of infrared Fluxes for clear Sky

Equations (14) and (16) are used to calculate the flux of IR radiation for CO_2, CH_4, NO_2, O_3, F-11 and F-12. For these gases the band absorptance $\int A_{\nu i} \mathrm{d}\nu$ is given by the corresponding band spectral interval $\Delta\nu_i$. For these gases A_ν is estimated by it's value at the center of the spectral interval, and we thus assume that theses interval are narrow enough. (see figure 15)

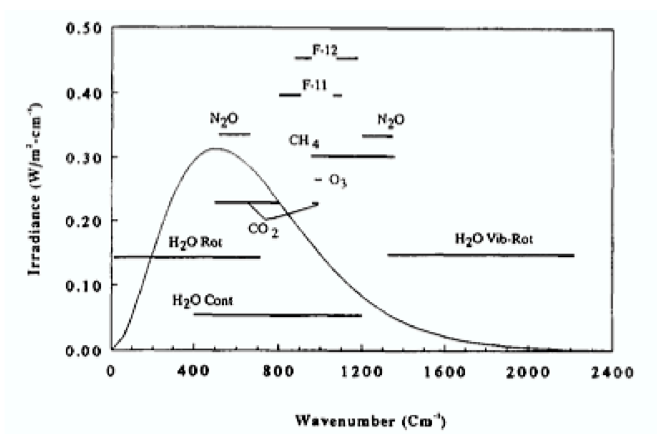

Figure 15: Significant absorbers of terrestrial radiation and their spectral ranges. Also shown is the relative black body irradiance for a black body at 260 K.

Fo water vapor this approximation is not possible anymore and for IR flux calculations involving water vapor, equations (17) and (15) are used. Moreover [MacKay 91] cited that for water vapor this emissivity data was more easily available. If we consider an atmosphere with water vapour and N other atmospheric gases the upward flux of IR radiation at level z is given by:

$$F^{\uparrow} = \sigma\, T^4(0) + \int_0^z \epsilon'_{\mathrm{H_2O}}(z,z')\, \frac{\mathrm{d}[\sigma\, \mathrm{T}^4(\mathrm{z}')]}{\mathrm{d}\mathrm{z}'}\, \mathrm{d}\mathrm{z}' + \sum_{\mathrm{i}=1}^{\mathrm{N}} \int_0^{\mathrm{z}} \mathrm{A}_{\nu\mathrm{i}}(\mathrm{z},\mathrm{z}')\, \Delta\nu_{\mathrm{i}}\, \frac{\mathrm{d}[\pi\, \mathrm{B}_{\nu\mathrm{i}}(\mathrm{z}')]}{\mathrm{d}\mathrm{z}'}\, \mathrm{d}\mathrm{z}'.$$

We thus see that the surface is considered to be a perfect black body and the emissivity (approximately 0.97 for the ocean) is neglected. However this approximation is negligible because the model is used to calculate differences in equilibrium temperatures. The downward flux for the same atmosphere is:

$$F^{\downarrow} = \lim_{z' \to \infty} \sigma T^4(z_t)\, \epsilon'_{H_2O}(z,z') + \int_{z_t}^{z} \epsilon'_{H_2O}(z,z') \frac{\mathrm{d}[\sigma\, \mathrm{T}^4(\mathrm{z}')]}{\mathrm{dz}'} \mathrm{dz}' + \\ + \sum_{i=1}^{N} \left\{ \lim_{z' \to \infty} \pi\, B_{\nu i}(z_t)\, A_{\nu i}(z,z')\, \Delta\nu_i + \int_{z_t}^{z} A_{\nu i}(z,z')\, \Delta\nu_i \frac{\mathrm{d}[\pi\, \mathrm{B}_{\nu \mathrm{i}}(\mathrm{z}')]}{\mathrm{dz}'} \mathrm{dz}' \right\}.$$

4.1.5 Infrared fluxes for cloudy Sky

The 1DRCM model includes one cloud layer. The cloud fully occupies the layer vertically and covers a fraction A_c in the horizontal direction. The cloud is assumed to be a perfect blackbody for infrared radiation. The net upward flux of infrared radiation is calculated as:

$$F^{\uparrow} = A_c F^{\uparrow}_{\text{cloud}} + (1 - A_c) F^{\uparrow}_{\text{clear}}, \tag{18}$$

where, $F^{\uparrow}_{\text{clear}}$ is calculated as described in 4.1.4, and $F^{\uparrow}_{\text{cloud}}$ is given by:

$$F^{\uparrow}_{\text{cloud}} = F^{\uparrow}_{\text{clear}} \qquad \text{if} \quad z \le z_{kap+1},$$

$$F^{\uparrow}_{\text{cloud}} = \sigma T^4(kap) + \int_{z_{kap}}^{z} \epsilon'_{H_2O}(z,z') \frac{\mathrm{d}[\sigma\, \mathrm{T}^4(\mathrm{z}')]}{\mathrm{dz}'} \mathrm{dz}' \\ + \sum_{i=1}^{N} \int_{z_{kap}}^{z} A_{\nu i}(z,z')\, \Delta\nu_i \frac{\mathrm{d}[\pi\, \mathrm{B}_{\nu \mathrm{i}}(\mathrm{z}')]}{\mathrm{dz}'} \mathrm{dz}' \qquad \text{if} \quad z \ge z_{kap}.$$

$T(kap)$ represents the temperature of the top of the cloud layer, and z_{kap} and z_{kap+1} represent respectively the altitude of the top and bottom of the cloud layer. If the cloud layer would cover 100% of the sky, the cloud layer would act as surface for the upward flux.

The net downward flux is calculated in a similar way:

$$F^{\downarrow} = A_c F^{\downarrow}_{\text{cloud}} + (1 - A_c) F^{\downarrow}_{\text{clear}},$$

where, $F^{\downarrow}_{\text{clear}}$ is calculated as described in 4.1.4, and $F^{\downarrow}_{\text{cloud}}$ is given by:

$$F^{\downarrow}_{\text{cloud}} = F^{\downarrow}_{\text{clear}} \qquad \text{if} \quad z \ge z_{kap},$$

$$F^{\downarrow}_{\text{cloud}} = \sigma T^4(kap+1) + \int_{z_{kap+1}}^{z} \epsilon'_{H_2O}(z,z') \frac{\mathrm{d}[\sigma\, \mathrm{T}^4(\mathrm{z}')]}{\mathrm{dz}'} \mathrm{dz}' \\ + \sum_{i=1}^{N} \int_{z_{kap+1}}^{z} A_{\nu i}(z,z')\, \Delta\nu_i \frac{\mathrm{d}[\pi\, \mathrm{B}_{\nu \mathrm{i}}(\mathrm{z}')]}{\mathrm{dz}'} \mathrm{dz}' \qquad \text{if} \quad z \le z_{kap+1}.$$

4.1.6 Absorption of solar Radiation

A description of the physics involved in the absorption and scattering of solar radiation can be found in appendix A

The absorption of solar radiation is calculated following [**Lacis 74**]. They state that there are two principal absorbers in the earth's atmosphere, namely water vapour in the near-infrared region and ozone in the ultraviolet and the visual band. This implies that all the other other gases(mainly CO_2, but also O_2, NO_2, N_2O and CH_4) that absorb solar radiation are not taken into considerations in the model. [Lacis 74] indicate that $CO_2$and O_2 are together responsible for $\approx 2.5\%$ of the absorption in the atmosphere-surface system, and thus identifying them as minor absorbers.

We will first give the absorption of visual light by ozone in the Chappius band, which can to a in good approximation, be given by:

$$A^{\text{vis}}_{\text{O}_3}(x) = \frac{0.02118 \cdot x}{1 + 0.042 \cdot x + 0.000323 \cdot x^2},$$

where x is the amount of ozone in cm-STP[42]. The fit for the ultraviolet absorption is:

$$A^{\text{uv}}_{\text{O}_3}(x) = \frac{1.082 \cdot x}{(1 + 138.6 \cdot x)^{0.805})} + \frac{0.0658 \cdot x}{1 + (103.6 \cdot x)^3}.$$

The total absorption is thus given by:

$$A_{\text{O}_3}(x) = A^{\text{vis}}_{\text{O}_3}(x) + A^{\text{uv}}_{\text{O}_3}(x).$$

The diffuse radiation illuminating level l from below is given in the model by:

$$x^{\downarrow}_l = u_l M,$$

where u_l is the total ozone amount (cm-STP) above the considered layer and M is a magnification factor, which accounts for the slant path of the ray as well as the refraction. It is given by:

$$M = \frac{35}{\sqrt{1224\mu_0^2 + 1}},$$

where μ_0 is the cosine of the zenithal angle of the sun. We denote the total ozone amount above the main reflecting level, which is in this case the cloudtop level, by u_t. Then the diffuse radiation illuminating level l from below is parametrised as:

$$x^{\uparrow}_l = u_t M + \overline{M}(u_t - u_l),$$

where $\overline{M}$ is the effective magnification factor for a diffuse upward radiation. [Lacis 74], have determined this factor to be $\overline{M} = 1.9$, which is the value for the best fit in a least-squares sense to multiple-scattering results for a clear sky and a zenithal angle of 60°.

For the ozone absorption it is considered that the atmosphere consists of two regions. The higher one is purely absorbing and the lower one is reflecting. Both are begin separated by the cloudtop. This implies that the absorption at level l consists of a contribution form the incoming radiation, and a contribution due to the reflected radiation (term in square brackets):

$$A_{l,\text{oz}} = \mu_0\{A_{\text{O}_3}(x^{\downarrow}_{l+1}) - A_{\text{O}_3}(x^{\downarrow}_l) + \overline{R}(\mu_0)[A_{\text{O}_3}(x^{\uparrow}_l) - A_{\text{O}_3}(x^{\uparrow}_{l+1})]\},$$

where $\overline{R}(\mu_0)$ is the albedo of the reflecting region, which can be evaluated in terms of the effective albedo of the lower atmosphere $\overline{R_a}(\mu_0)$, and the ground reflectivity R_g:

$$\overline{R}(\mu_0) = \overline{R_a}(\mu_0) + \frac{[1 - \overline{R_a}(\mu_0)](1 - \overline{\overline{R_a}})R_g}{1 - \overline{\overline{R_a}}R_g}$$

[42]for definition see section 4.2.1.

where $\overline{\overline{R_a}}$ is the average of $\overline{R_a}(\mu_0)$ over all sun angles. [Lacis 74] have fitted this parametrisation to the multiple scattering method in a least-square sense and found that for a a cloudy sky we can take:

$$\overline{R_a}(\mu_0) = \overline{\overline{R_a}} = \frac{\sqrt{3}(1-g)\tau^c}{2+\sqrt{3}(1-g)\tau^c},$$

where τ^c is the total visual optical thickness of the clouds and g is the asymmetry factor for the cloud particle phase function.

Absorption by water vapour consists the major source of solar radiative heating in the atmosphere. However this absorption is impossible to parameterise for a cloudy sky, and it is calculated by an adding method[43], in which it is assumed that all radiation reflected or transmitted by a cloud are diffused with an average magnification factor of 5/3.

4.1.7 Temperature of each Layer

The model uses a time stepping procedure to calculate the average temperature change at_i of each layer. This change is divided into a IR heating rate and a heating rate due to absorbed solar radiation. The first one is given by:

$$\left(\frac{\Delta at_i}{\Delta t}\right)_{\mathrm{I}} = \left(\frac{g}{(C_p^*)_i}\right)\left(\frac{\Delta F_i}{\Delta P_i}\right), \tag{19}$$

where at_i is the average temperature of layer i, Δt is the time interval of each step, g is the is the acceleration of gravity, $(C_p)_i$ is the effective specific heat capacity of each layer, $F = F^{\uparrow} - F^{\downarrow}$ is the net upward flux of IR radiation, as calculated in section 4.1.4, and ΔP is the pressure difference between the top and the bottom of the layer. The effective specific heat capacity is given by:

$$C_p^* = C_p + L\frac{\partial q}{\partial T},$$

where L is the latent heat of vaporisation given by: $L = 2510 - 2.38(T - 273)$, C_p is the specific heat of dry air, q is the absolute humidity of the air and T its temperature.

On the other hand the heating due to absorbed solar energy is given by:

$$\left(\frac{\Delta at_i}{\Delta t}\right)_{\mathrm{Q}} = \left(\frac{g}{(C_p^*)_i}\right)\left(\frac{A_i}{\Delta P_i}\right), \tag{20}$$

where A_i is the the net flux of solar energy absorbed by layer i.

As was already mentioned when the general structure of the model was described, in this model the Earth's surface is assumed to be a throughly mixed layer of water of uniform depth h. The change in surface temperature Δat_{19} is calculated according to:

$$c_w \rho h(\Delta at_{19}) = [F_{19}^{\downarrow} + A_{19} - \sigma(at_{19})^4] \cdot \Delta t,$$

where c_w is the specific heat of water ,ρ its density and σ is Stefan's constant. $F_{19}^{\downarrow}$ and A_{19} are as previously the downward flux of IR radiation at the surface and the absorbed flux of solar radiation at the surface respectively.

This time stepping procedure is repeated until equilibrium is reached, i.e. the net solar energy absorbed by the earth atmosphere system is equal to the IR radiation given off by the earth atmosphere system back into space.

The temperatures at the top and the bottom of the layers are calculated as pressure weighted averages. They are used to estimate the derivatives of functions with respect to temperature at the centre of each layer. The same is true for pressures of the top and bottom of each layer.

[43] refer to [Lacis 74] for a detailed description of this method

4.1.8 Vertical Profile of Water Vapour

The vertical profile of relative humidity h used in the model is given by:

$$h = h' \left(pa_i - (0.02/0.98)\right),$$

where h' is the surface relative humidity taken to be 0.77. This equation is used for each layer except the layer containing a cloud for which $h = 1$. The specific humidity q is given by:

$$\begin{aligned} q = 0.622\, h\, e_s(T)/(pa_i - h\, e_s(T)) \quad &\text{if} \quad q > 3 \cdot 10^{-6}, \\ q = 3 \cdot 10^{-6} \quad &\text{if} \quad q \leq 3 \cdot 10^{-6}, \end{aligned}$$

where pa_i is the average pressure of layer i, e_s is the saturated vapour pressure. We thus see that the minium value of q is taken to be $3 \cdot 10^{-6}$.

4.1.9 Vertical Profile of other Gases

The model includes several other greenhouse gases than water vapour. The CO_2 concentration is constant with altitude for all levels of the model. Furthermore the model includes NO_2 and CH_4, whose analytical profiles have been calculated to fit the values of measured profiles. The vertical distribution of ozone (before the perturbation added below) is based on the standard atmosphere of the National Climate Center of NOAA. Finally the model also includes chlorofluorocarbons (F-11,F-12). As for carbon dioxide their concentration is assumed to be constant with altitude.

4.1.10 Convective Adjustment

At every time step the temperature for every layer due to radiative heating (or cooling) is calculated, as was explained in section 4.1.7. The model then calculates the lapse rate between the first two layers of the model. If this lapse rate exceeds a critical value [44], a convective adjustment is performed. This is performed by removing energy from the lower layer and increasing the temperature of the upper layer. This procedure is repeated for every pair of layers in the model up to the layer which contains the troposphere. The whole process is repeated several times if necessary until all lapse rates are under the critical level.

In order to maintain the energy constant in the model, an amount of energy is removed from the surface equal to the net increase in energy of all atmospheric layers due to the adjustment process.

4.2 Including aircraft-induced Changes in the Model

As mentioned at the beginning of section 4.1, the 1DRCM model was initially designed to evaluate the impact of greenhouse gases on global mean temperature. The model had thus to be changed considerably to evaluate the impact of aircraft on climate change in Europe.

4.2.1 Greenhouse Gases pertubated by Aviation

CO_2 and CH_4, are long-lived greenhouse gases whose concentrations are altered by aviation. Their long lifetime implies that these two gases are uniformly distributed on a vertical and horizontal scale. It is thus sufficient to increase the global concentration of the gas. The amount of this increase is given in the next chapter.

[44]This value is set to be 6.5 K/km in the model for all levels, but this value is subject of discussion (see [MacKay 91], p. 396)

On the other hand, the emission of NO_x, induces an increase in ozone, but this increase presents an important peak at the main cruising altitude of airliners, at around 10 km. Most inventories give the increase in concentration of O_3 as a function of altitude. However the 1DRCM uses an ozone distribution that is given in cm-STP[45] , and will derive now a formula to transform the concentration in ppmv to cm-STP.

To do this we consider a column of air containing a given vertical distribution of the concentration of ozone $C_{O_3}(p)$ as a function of pressure-altitude. If the concentration is expressed in ppmv we have:

$$C_{O_3}(p) = \frac{n_{O_3(p)}}{n_{air(p)}} \cdot 10^6, \tag{21}$$

where $n_{O_3(p)}$ and $n_{air(p)}$ are respectively the number of molecules of ozone and of air at pressure altitude p.

As the air can be considered to be an ideal gas we may write: $pV_{air}(p) = N_{air}(p)RT$, where V_{air} is the volume occupied by $N_{air}(p)$ the number of molecules of air at pressure p and temperature T. R is the perfect gas constant. We can write the same relation for ozone: $pV_{O_3}(p) = N_{O_3}(p)RT$, with the obvious definition of variables. As both gases are for a given altitude at the same pressure and temperature, we may write:

$$\frac{V_{air}(p)}{V_{O_3}(p)} = \frac{h_{air}(p)S}{h_{O_3}(p)S} = \frac{N_{air}(p)}{N_{O_3}(p)} = \frac{n_{air}(p)N_a}{n_{O_3}(p)N_a} = \frac{1}{C_{O_3}(p) \cdot 10^{-6}},$$

where S is the surface of the column of air, $h_{air}(p)$ the height of the column of air, $h_{O_3}(p)$ that of the column of ozone and N_a is the number of Avogrado. From these relations we deduce that for any pressure level p we have:

$$h_{O_3}(p) = C_{O_3}(p) \cdot 10^{-6} h_{air}(p).$$

As the amount of ozone at altitude p expressed in cm-STP, includes by definition the total concentration above that level we integrate from the top of the atmosphere (where $p = 0$) to the level p:

$$\int_0^p h_{O_3}(p')\mathrm{d}p' = \int_0^p C_{O_3}(p') \cdot 10^{-6} h_{air}(p')\mathrm{d}p'.$$

Moreover by definition of the cm-STP the whole atmosphere is considered to be at STP. In that case $h_{air}(p') = 799500$cm and the first integral yields h_{O_3} when the pressure is expressed in atm:

$$h_{O_3}(p) = \int_0^p C_{O_3}(p') \cdot 0.7995\, dp', \tag{22}$$

where $C_{O_3}(p')$ is expressed in ppmv and p and p' in atm.

In chapter 5 the vertical distribution of the ozone perturbation due to aviation will be given.

4.2.2 Adding Soot and Sulfate Aerosols to the Model

For his final year project Régis Tonneau already added a layer of aerosols to the model [Tonneau 02]. His code will be used and we will give here a short overview of the working method. This section only considers the direct impact of aerosols, as explained in chapter 1. The indirect effect namely, the impact on clouds, is not evaluated in this work.

The direct impact of sulfate aerosols is to scatter incoming radiation, and thus they raise the radiation backscattered to space. On the other hand soot particles absorb primary radiation and there is nearly no scattering.

[45] An ozone layer which has a thickness of 1cm-STP will occupy a layer that has a height of 1cm in an atmosphere at standard temperature and pressure (STP)

The following hypotheses were emitted in order to estimate the direct forcing of these aerosols in the atmosphere:

- The layer is supposed to be optically thin ($\tau \ll 1$). This is a very good approximation for the aerosols emitted by airliners.(see section 5.2.3)
- Aerosols are supposed to be spherically symmetric, in order to be able to apply Mie diffusion (see appendix A for a physical description of this theory). Soot particles emitted by aircraft are in fact composed of nearly spherical particles. ([IPCC 99] p. 75)
- The particles are supposed to be hydrophobic. In this way their optical properties (i.e. size and refraction indices) are not altered. This approximation seems rather crude for particles in the plume of an aircraft. ([IPCC 99] p.73)

The contribution of a layer of aerosols on radiative forcing is given by the change of the albedo of the combined system formed by the surface and the aerosol layer. This is given by [Tonneau 02]:

$$H_{\text{aero}} = -\frac{S_0}{4} T_{\text{atm}}^2 (1 - A_c) \Delta R,$$

where $S_0/4$ is the incident global solar radiation at the top of the atmosphere (342 W·m^{-2}, T_{atm} the transition coefficient of the atmosphere below the aerosol layer (≈ 0.75), A_c is the fraction of cloud covered by the cloud layer, and ΔR is the change is surface albedo due to the presence of a layer of aerosols.

Using multiplying reflection of radiation between the surface layer and the ground, [Russell 97] showed that this increase in albedo could be given by:

$$\Delta R = \omega \frac{\tau}{\mu} \left[\beta(\mu) \, (1 - R_s) - 2 \, \mu \, \bar{\beta} \, R_s \, (1 - R_s) \right] - (1 - \omega) \frac{\tau}{\mu} R_s \, (1 - 2 \, \mu),$$

with ω the simple diffusion albedo, τ the optical thickness of the aerosol layer,μ is the cosine of the zenithal angle, $\beta(\mu)$ is the fraction of the incident radiation of direction μ that is being backscattered, R_s the surface albedo below the aerosol layer and $\bar{\beta}$ is the mean of $\beta(\mu)$ over all incident angles.

Table 7 gives the different parameters for sulfate aerosols and for soot [Tonneau 02]. The model gives us the zentihal angle, and thus we only need to determine the optical thickness τ of the layer of aerosols.

	SO_4^{--}	Soot
ω	1.0	0.21
$\bar{\beta}$	0.22	0.38

Table 7: Parameters for different aerosols

4.3 Adapting the Model to European Climate

In order to be able to compare the results we will derive in chapter 5 with later results derived by MAR, we will use a region extending from 35° N to 60° N, and from 30° W to 30° E. Figure 16 shows the domain that is used for MAR[46] in Western Europe. The two domains do not coincide exactly, but are close enough for comparisons to be possible.

[46]MAR (*Modèle Atmosphérique Régional*) is a regional atmospheric model used at the *Institut Georges Lemaître* at UCL, to study different regional impacts.

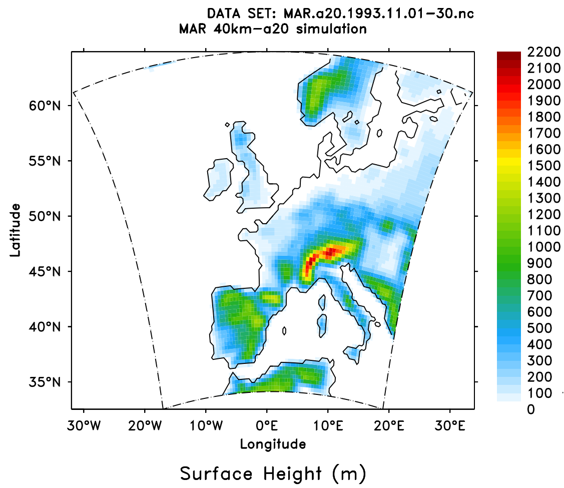

Figure 16: European domain used in MAR (personal communication from Vanvyve Emilie)

4.3.1 Changing the Flux of solar Radiation

As the one dimensional model used was originally designed to work on a global average, the instantaneous flux of solar radiation in the model has to be cahnged, which at any point on the globe can be given by [Sellers 65]:

$$Q_s' = S\left(\frac{\bar{d}}{d}\right)^2 \cos Z, \tag{23}$$

where S is the solar constant[47], $\bar{d}$ the mean distance between the sun and the earth[48], d is the actual distance to the sun, and Z is the zenithal angle. Knowing the declination δ[49], as well as its hour angle h[50] for a given latitude ϕ, the zenithal angle is given by:

$$\cos Z = \sin\phi\sin\delta + \cos\phi\cos\delta\cos h. \tag{24}$$

For any latitude except at the poles the sunset or sunrise occurs when $\cos Z = 0$, and thus the half-day length H, is given by:

$$\cos H = -\tan\phi\tan\delta.$$

In order to determine the daily total solar radiation incident on o horizontal surface at the top of the atmosphere, we introduce (24) into (23), and integrate from sunrise to sunset:

$$Q_s = \int_{-H}^{H} Q_s'\,\mathrm{dt} = \mathrm{S}\left(\frac{\bar{\mathrm{d}}}{\mathrm{d}}\right)^2 \int_{-\mathrm{H}}^{\mathrm{H}} (\sin\phi\sin\delta + \cos\phi\cos\delta\cos\mathrm{h})\mathrm{dt}.$$

[47] The solar constant is defined to be the flux of solar radiation at the outer boundary of the earth's atmosphere that is received on a surface perpendicular to the sun's direction at the mean distance between the sun and the earth.

[48] The mean distance, or astronomical unit, is defined as the distance from the Sun at which a particle of negligible mass, in an unperturbed circular orbit, would have an orbital period of a Gaussian year.

[49] The declination of the sun is of the sun the angular distance of the sun relative to the equator

[50] The hour angle at a given latitude is the angle through which the earth must turn to bring the meridian under the sun.

Remarking that $\frac{\mathrm{dh}}{\mathrm{dt}} = \omega$, the angular velocity of the earth of 2π rad per day, we deduce that:

$$Q_s = \frac{S}{2\pi}\left(\frac{\bar{d}}{d}\right)^2 (H \sin\phi \sin\delta + \cos\phi \cos\delta \sin H).$$

The factor $(\bar{d}/d)^2$ is very close to unity, it is ranging from 1.0344 in January to 0.974 in July.

4.3.2 Changing the Surface Albedo

[Sellers 65] gives in Table 3 on p.29 values of surface albedo for North America, in winter and in summer. As for western Europe there is the influence of the Gulf Stream, which induces a higher surface temperature in winter than over the North-American continent, we decided to adopt the values of light snow cover for January, for which the mean albedo between 35°N and 60°N is 32.8%. For the summer months the same mean albedo is 15.64%.

4.3.3 Taking horizontal Fluxes into Account

As explained in section 4.1.7 the temperature change for each layer in the model is divided into a IR heating rate ($(\Delta at_i)_{\mathrm{I}}$) and a heating rate due to absorbed solar radiation ($(\Delta at_i)_{\mathrm{Q}}$). In the real atmosphere the temperature change Δat_i experienced by a column of air at a given latitude is furthermore due to:

- $(\Delta at_i)_{\mathrm{H}}$, the vertical transfer of sensible heat from the ground or ocean,
- $(\Delta at_i)_{\mathrm{C}}$, the net horizontal transfer of sensible heat into the column from the surroundings,
- $(\Delta at_i)_{\mathrm{L}}$, the net release of latent heat.

Which results in the mathematical expression:

$$(\Delta at_i) = (\Delta at_i)_{\mathrm{Q}} + (\Delta at_i)_{\mathrm{I}} + (\Delta at_i)_{\mathrm{H}} + (\Delta at_i)_{\mathrm{C}} + (\Delta at_i)_{\mathrm{L}}. \tag{25}$$

Similar to equations (19) and (20), the temperature change due to a net heat flux Q_i at level i is given by ([Sellers 65], pp. 32):

$$\left(\frac{\Delta at_i}{\Delta t}\right) = \left(\frac{g}{(C_p^*)_i}\right)\left(\frac{Q_i}{\Delta P_i}\right).$$

We may thus rewrite equation (25):

$$(G_a)_i = A_i - \Delta F_i + H - \Delta C_i + (Lr)_i, \tag{26}$$

where, G_a is the net storage rate of the atmosphere, A and F are respectively the net flux of solar energy absorbed and the net upward flux of IR radiation, as defined in section 4.1.7. H is the sensible heat flux from the ground, ΔC is the flux of sensible heat from the surroundings, and L is the net rate at which the water vapor is condensed in the column, which is approximated by r the precipitation rate (see [Sellers 65] pp.119).

Figure 17 gives the distribution of these different fluxes as a function of the latitude. For a European latitude of 50°N we see that ΔC can be neglected compared to H and Lr. The sum of H and Lr gives an additional forcing of approximately 80 Wm^{-2}.

In order to get a realistic surface temperature for Europe, we introduced this forcing at the ground level into the model[51]. Although the latent heat of condensation does not take place

[51] We may here interfere that in this approach the zonal fluxes that are present in and out of a box over Europe are forgotten. However this addition flux of 80 Wm^{-2}gave a temperature that was nearly identical with the temperature form the IPCC Datacenter, and we may thus conclude that on an annual mean the zonal fluxes are negligible, but this hypothesis could not be verified.

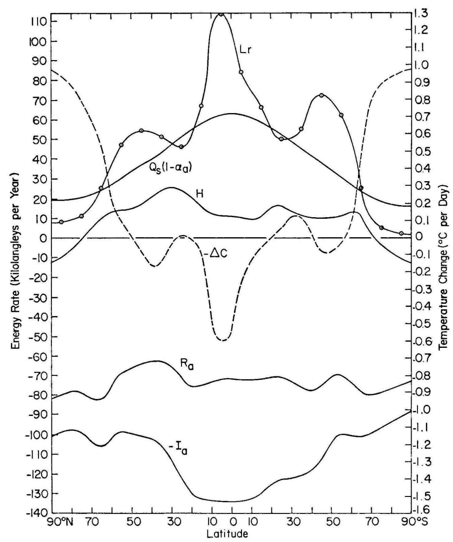

Figure 17: The average annual latitudinal distribution of the components of the energy balance of the atmosphere. $Q_s(1-\alpha_a)$ corresponds to the heating rate of solar radiation, where α_a is the albedo of the atmosphere, I_a is the effective outgoing radiation form the atmosphere, and R_a is the radiative balance of the atmosphere, given by: $R_a = Q_s(1-\alpha_a) - I_a$. (One kiloLangely per year corresponds to 1.33 Wm^{-2}) (from [Sellers 65])

near the ground, we decided to introduce it at that level so as not to increase the complexity of the model too much.

The model was then equilibrated by changing this flux for the different runs (year, January, July) to give the surface temperaure averaged over 1901 – 1995 period in Europe which was extracted from IPCC Datacenter.

4.3.4 Background Atmosphere

Tables 8 and 9 give the concentrations of the greenhouse gases in the atmosphere without perturbation from aviation for model runs on a global mean as well as in Europe. Table 8 and 9 give the cloud cover and the surface albedo for the different situations.

The values for carbon dioxide, methane and ozone background concentrations were taken from [IPCC 99] were the IS92a scenario was used, in order to get comparable results. The cloud cover was taken from IPCC Datacenter and the surface albedo from [Sellers 65].

	Global					
	2002			2025		
	Year	**January**	**July**	**Year**	**January**	**July**
CO_2(ppmv)	375.6			432		
CH_4(ppmv)	1.832			2.242		
N_2O (ppmv)	0.3208			0.344		
O_3(DU)	295	293	300	301	299	306
cloud cover (%)	63.6	64.0	62.2	63.6	64.0	62.2
surface albedo (%)	13					

Table 8: Background atmosphere for the World

	Europe					
	2002			2025		
	Year	**January**	**July**	**Year**	**January**	**July**
CO_2(ppmv)	375.6			432		
CH_4(ppmv)	1.832			2.242		
N_2O (ppmv)	0.3208			0.344		
O_3(DU)	301	288	308	307	294	315
cloud cover (%)	63.2	73.4	51.4	63.2	73.4	51.4
surface albedo (%)	13	31.8	15.5	13	31.8	15.5

Table 9: Background atmosphere for Europe

CHAPTER V
Results and Interpretation

In this chapter we will first give some preliminary results that were obtained to test how the model responds to different forcings. Next we will give the way in which changes in radiatively substances were derived from the emissions given by AERO2k. Finally we will present and discuss the results obtained with the one dimensional model for perturbations due to aviation.

5.1 Preliminary Results

We will begin by investigating the sensitivity to a doubling of the CO_2 concentration. Next we will test the influence of the altitude of an ozone perturbation and we will make a similar experiment for a soot and a sulfuric aerosol layer.

5.1.1 Carbon Dioxide Doubling

When doubling the concentration of carbon dioxide in the model a surface temperature increase of 1.95 K is observed, which is in the lower part of the range given by IPPC for this doubling (1.5 to 4.5 K)[52]— which is known as climate sensitivity. Thus the figures derived from other models and in reality could be higher than those that will be presented in this chapter.

This rather low climate sensitivity is essentially due to the fact that this simple model is missing some important feedback processes, particularly related to water vapour, since humidity and clouds doen't respond to temperature and convection. Moreover ice-albedo feedbacks, biophysical (vegetation) feedbacks and others are also missing.

5.1.2 Influence of Altitude of Ozone Pertubation

In order to get the influence of the altitude of an ozone perturbation on the change of surface temperature, we introduced a layer of ozone that has a thickness of 10 DU[53] into the model. Figure 18 gives the temperature increase when the layer is at different altitudes in the model. Thus we see that the temperature increase is biggest when the layer is at the tropopause. This

[52]since IPCC-TAR this climate sensitivity has been a topic of many further studies, and the general conclusion is that it is probably higher — less than 2°C has been found to be inconsistent with the observed history of temperature change, whereas up to 8°C is physically possible in GCMs and cannot be ruled out by consistency with palaeo records

[53]This thickness was chosen arbitrarily, and has no relation to the pertrubations due to airliners

result was predictable from a point of view of radiation [54] because the temperature is lowest at this point of the atmosphere. In fact this implies that the difference of energy associated to the absorption of radiation emitted by the surface and the emissions of the black body associated to the local temperature is most important at the tropopause. The nonlinear behaviour above the troposphere is due to the fact that the equilibrium temperature of the model is not increasing uniformily through the stratosphere.

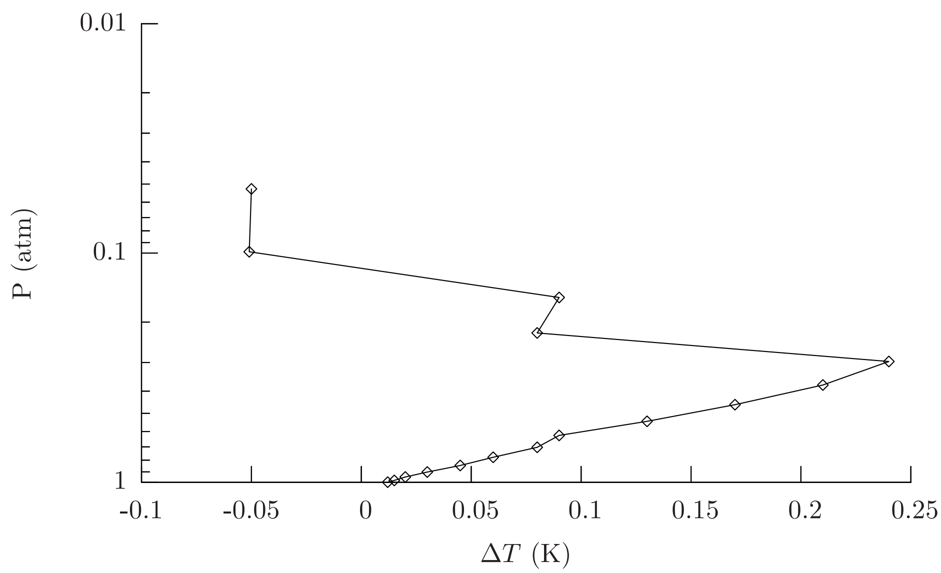

Figure 18: Surface Temperature change (ΔT) due to a ozone layer with a thickness of 10 DU, as a function of pressure (P) altitude of the layer — from 1DRCM

[**Hansen 97**] have performed a similar result with a simpilfied GCM. They have used a layer of 100 DU thickness, and obtained an maximal increase of 2.36 K which is in accordance with the results obtained (it has been verified that the response of the model is linear to the optical thickness of the layer). However on figure 19 we can see that the increase is not so located at the tropopause but more spread out compared to our results. This is due to the fact that their model includes feedback processes that are missing in the 1D model, as is evident from the variation in lambda with altitude

The λ parameter in graph 19 is defined by:

$$\lambda = \frac{\Delta T_s(\text{ozone forcing})}{\Delta T_s(\Delta \text{S}_0 \text{ forcing})}.$$

It gives the factor of the surface temperature change due to the ozone layer, compared to the surface temperature change due to a spectrally uniform change in solar irradiance with the same radiative forcing than the ozone layer. [**Hansen 97**] stated that λ "should be near unity for all forcing if the adjusted forcing is a good predictor of climate response". As this factor varies considerably as a function of altitude for an ozone perturbation, this suggest that radiative forcing may not be the best indicator for climate change due to ozone created by aircraft.

[54] There are also photochemical considerations which imply that NO_xemitted at this altitude induces higher concentrations of ozone than in other parts of the atmosphere

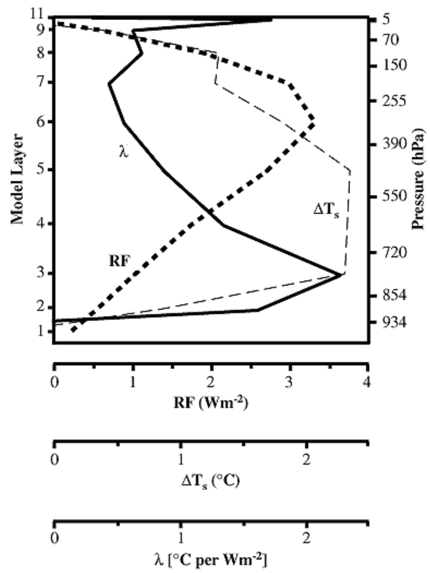

Figure 19: Radiative forcing (dotted line), global mean surface temperature change including all internal feedback processes (dashed line), and climate sensitivity parameter λ (solid line) from 100 DU additional ozone as a function of altitude (model layer) to which ozone was added. (from a GCM study by [Hansen 97])

5.1.3 Aerosols Experiments

We have done similar experiments with a layer of soot and a layer of sulfate aerosls wich were placed at different altitudes into the model. Figure 20 gives the results of these experiments. We can see that the temperature change due to sulfate aerosols reduces regularly as the altitude of the layer increases, whereas that due to soot aerosols are sensitive to their location relative to the tropopause. This can be explained by the way both types of aerosols perturbate the radiation balance.

Sulfate particles mainly scatter incoming sunlight thus increasing the albedo effect, but there is no absorption modeled. This explains why their effect is not sensitive to the environmental temperature. The effect is not uniform with altitude, because the optical thickness of the aerosol layer is held constant. As the different layers of the model have different heights, this implies that the total amount of aerosols is not constant for all the runs, which implies the observed decrease of the impact.

On the other hand soot aerosols primarily absorb sunlight and heat the local air and there is virtually no scattering. Thus for soot there is a negative solar radiative forcing that is countered by a positive long-wave forcing. And in the stratosphere the thermal contrast existing between the black body radiation emitted by the surface, and the one of the local temperature diminishes. This implies a reduction of the positive long-wave forcing, and explains the effect lessens above the tropopause and finally to becomes negative.

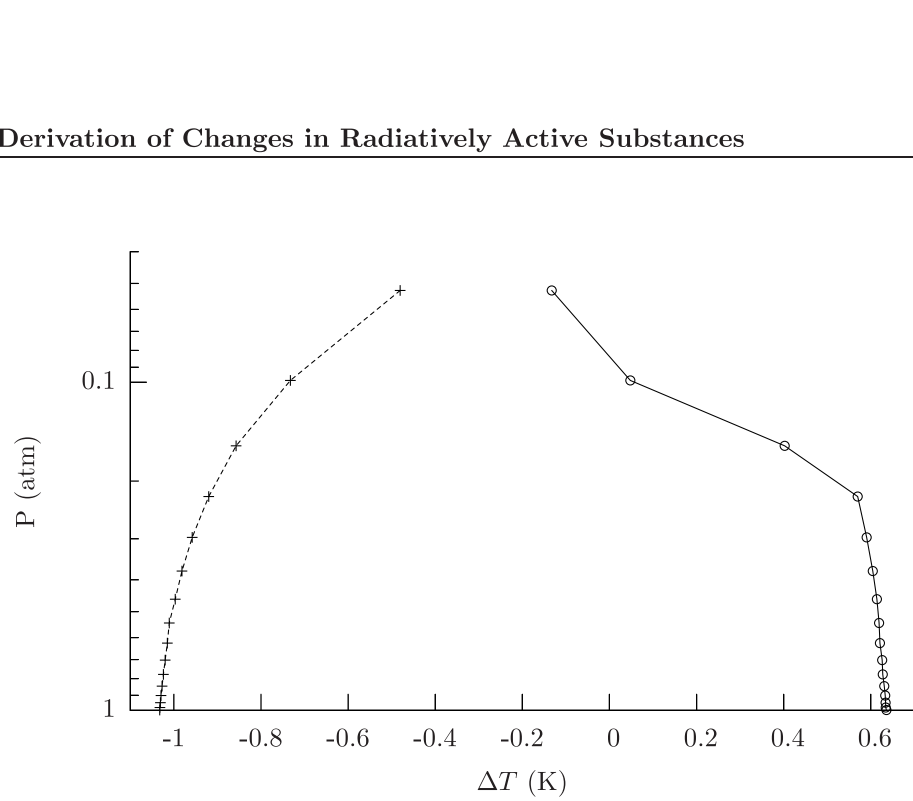

Figure 20: Surface Temperature change (ΔT) due to a soot layer (continuous line) and a layer of sulfate aerosols (dotted line), both of an optical thickness of 0.1, as a function of pressure altitude (P) of the layer

5.2 Derivation of Changes in Radiatively Active Substances

This section explains how we got the changes in carbon dioxide, methane, ozone, as well as for aerosols induced by aircrafts, from their emissions given by AERO2k.

5.2.1 Changes in long lived greenhouse Gases

The AERO2k comes in a gidded format of 1° by 1° and a vertical resultion of 500 feet. Files for every month of the year 2002 as well as for the projection year 2025 are available. A Java tool was developed in order to visualise the data. This tool was also used to be able to interpolate the data in order to fit it to the 18 layers of the one dimensional model, and to average it on a global mean, or over the European box given in section 4.3.

For carbon dioxide there is an accumulation effect in the atmosphere due to its lifetime of the order of the century. AERO2k gives a total emission for 2002 of 150 Tg C yr^{-1}, which is about 20 % lower than the prediction for 2000 in [IPCC 99][55] . Assuming that this difference was the same in the years between 1990 and 2002, we subtracted 20% from the marginal concentration increase of carbon dioxide from 1990 to 2000. This leads finally to a marginal CO_2 concentration due to aviation of 1.4 ppmv. Considering the uncertainties of the model explained in section 3.3.2, this value lies in the ranges of 1.3 to 1.5 ppmv.

NO_x emissions for 2002 are calculated to be of 2.24 Mt NO_2 yr^{-1}, which is also about 20% smaller than projected by [IPCC 99]. Assuming the decrease in concentration of methane is linear to NO_x emissions, we calculated a marginal concentration decrease due to aviation of −45.4 ppbv, by the same procedure as previously. As we will explain in section 5.2.2 there is

[54] The gridded data can be found on `http://www.cate.mmu.ac.uk/data_aero2k.asp`

[55] As mentioned in chapter 3 this difference would be smaller when another database would have been used, because AERO2k was the lowest one in the [UNFCCC 05] comparison.

a big uncertainty, due to the chemistry involved. Supposing the relative change as big as for ozone, the range goes from 18.5 ppbv to 63.6 ppbv.

5.2.2 Changes in Ozone Concentrations

For ozone concentrations it is important to use a vertical distribution of the changes in concentration because this greenhouse gas is not uniformily distributed throughout the atmosphere as explained in chapter 1. The most accurate way would be to use a 3D chemistry model to get the change in O_3 concentrations from the emission of NO_x given by AERO2k. As we are only trying to get an order of magnitude in this work, we decided to derive multiplying factors in order to derive the increase of ozone due to NO_x emssions.

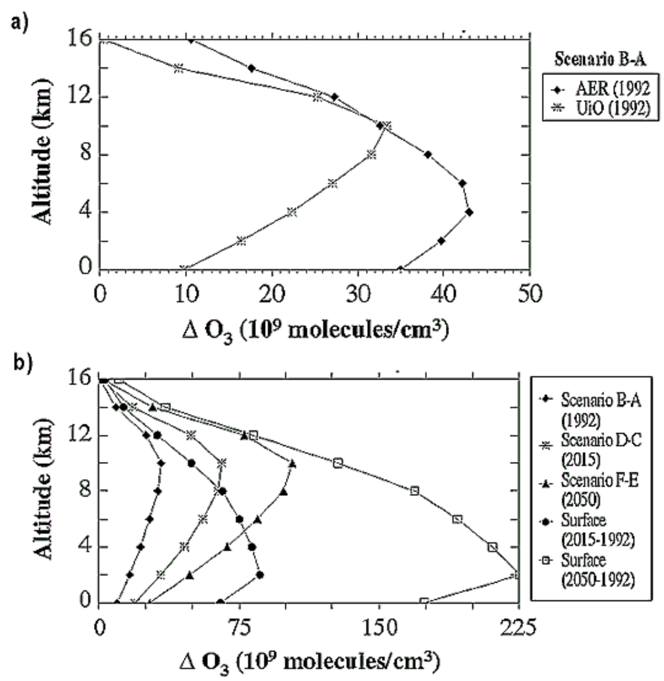

Figure 21: Annual average zonal mean change of ozone in the 30-60°N latitude band for various perturbations from UiO3D and AER2D models (from [IPCC 99])

Figure 21a gives the ozone increase due to aviation from a 3D model for the fleet of 1992. We assumed that the distribution of flight routes and the altitude of flights has not changed between 1992 and 2002. The idea isto compare the results from UIO3D to the vertical distribution of NO_x emitted, as given by AERO2k.

As the total emissions of NO_x are higher in 2002 than they were in 1992, we first scaled the vertical distribution of emissions from the 2002 fleet down to a total of 1.92 Mt NO_2 yr^{-1}, which is the total emitted by the 1992 fleet. These were then interpolated to the levels in figure 21a. Next we divided the change in ozone concentration given by figure 21a with this result, which gives us the multiplying factor as a function of altitude between NO_x and ozone on a global mean in the year 1992. Figure 22 shows the result of the interpolation of the multiplying factor to the levels of the 1DRCM model. It is important to note that we do not only account for the number of ozone molecules that are formed for one molecule of NO_x emitted but also the transport of these molecules in a vertical direction.

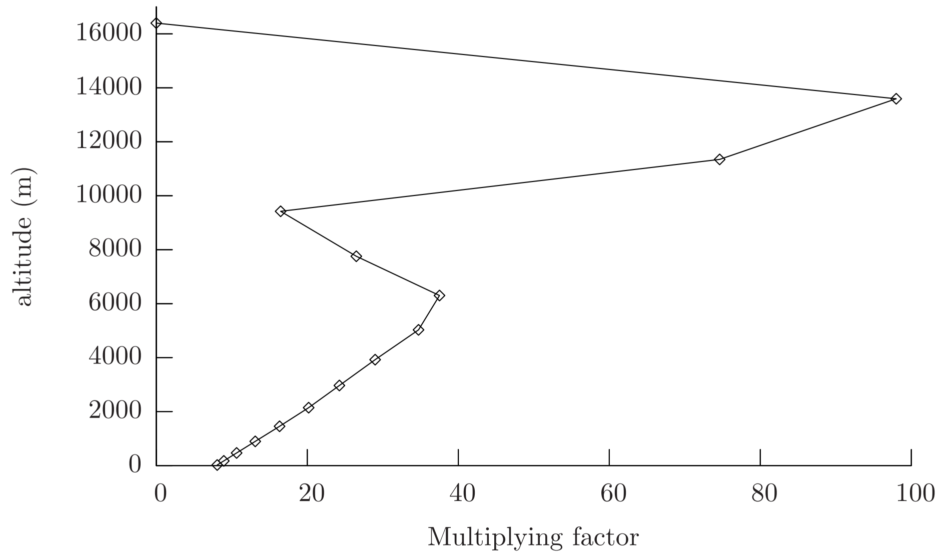

Figure 22: Multiplying factor (in molecules O_3produced per molecule of NO_xemitted) to get ozone concentration changes as a function of altitude

These ozone changes are subject to further uncertainties arising due to the modeling in the chemistry models. [Berntsen 03] gave an overview of the differences of the distribution and the maximum values of ozone perturbations for different models used for the TRADEOFF project. They can be seen in figure 23. In order to evaluate this uncertainty in our final results, we calculated additional multiplying factors in order to reach the highest and the lowest values of the different models. The multipying factor corresponding to find the highest model is of 1.4 and to the lowest one is of 0.26.

We used the same multiplying factors for all the runs, although as the chemistry involved is very sensitive to temperature changes, these factors are subject to change from one point on the globe to another, as well as in time. As our goal is to get only an order of magnitude of the changes, we considered this approximation to be not too bad.

5.2.3 Aircraft produced Aerosols

The AERO2k database gives the mass of soot produced, as well as an estimation of the particles emitted at the nozzle of the engines. For soot the total emission during 2002 is of 0.0039 Tg. This is very low compared to [IPCC 99], and the difference may be mainly attributed to the fact that AERO2k does not give an estimation for soot emitted by military planes or a different definition of soot.

[IPCC 99] gives the global soot column due to the perturbation for different tracer simulations (Table 3-4), and a back-scaling from the yearly emissions gives a global soot column of 0.065 ng cm^{-2}. As AERO2k does not include sulfate aerosols we decided to use the same back-scaling for the global SO_4 column given by [IPCC 99], which yield a column of 1.9 ng cm^{-2} for sulfate aerosols.

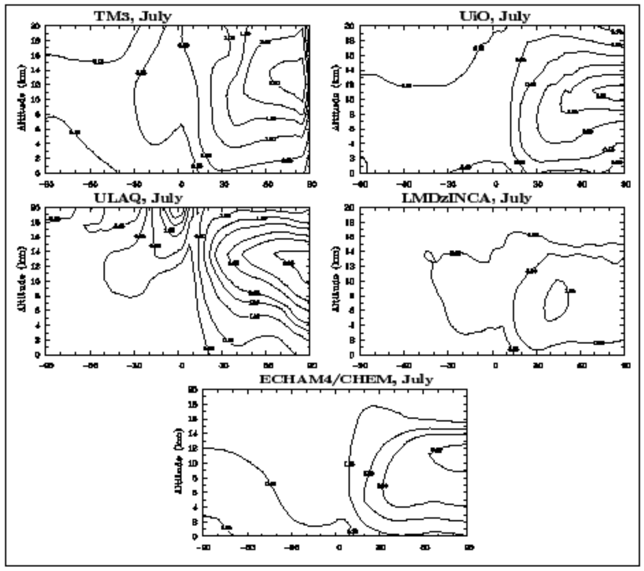

Figure 23: Zonally averaged ozone change (ppbv, July) due to aircraft emissions of NO_x.(from [Berntsen 03])

The optical depth of the aerosols is proportional to the column load. The sulfuric acid has a mass particle scattering efficiencies of 7 m^2g^{-1}, which gives us an optical thickness of $1.33 \cdot 10^{-4}$. On the other hand soot has mass extinction coefficient of about 10 m^2g^{-1}, and we thus get an optical thickness of $6.5 \cdot 10^{-5}$. (see [IPCC 99], p. 99)

From AERO2k we derived that air-traffic in Europe is about 5 times denser than on a global scale, and we deduced that the optical thicknesses are 5 times higher in Europe.

5.3 Description of the Results obtained with 1DRCM

First we will give the increase in surface temperature for the global aviation fleet in 2002 and 2025 as calculated with the one dimensional model and compare it with the results obtained in [IPCC 99]. In the following section we will give the results for the European domain as defined in chapter 3.3.2. Finally we will analyse the seasonal variation of the temperature increase due to aviation.

5.3.1 Global Surface Temperature change due to Aviation

Figure 24[56] gives us the increase of surface temperature for 2002 and 2025 due to aviation. We see that the total increase for 2002 is of 0.0128 K. [IPCC 99] uses 1990 as a basline year. A calculation with the model of the temperature increase for the 1990 fleet gives 0.0094K, and thus the difference of 0.0034K is in accordance with the figure of 0.004K as given by [IPCC 99]. For 2025 the increase with respect to 1990 is of 0.01978K which is slightly lower than the figure

[56]The error bars indicate the temperature range when the uncertainties were applied that have been explained in section 5.2. For the projection for 2025 it is important to note that AERO2k did not give an uncertainty on the scenario, and thus this uncertainty is not included

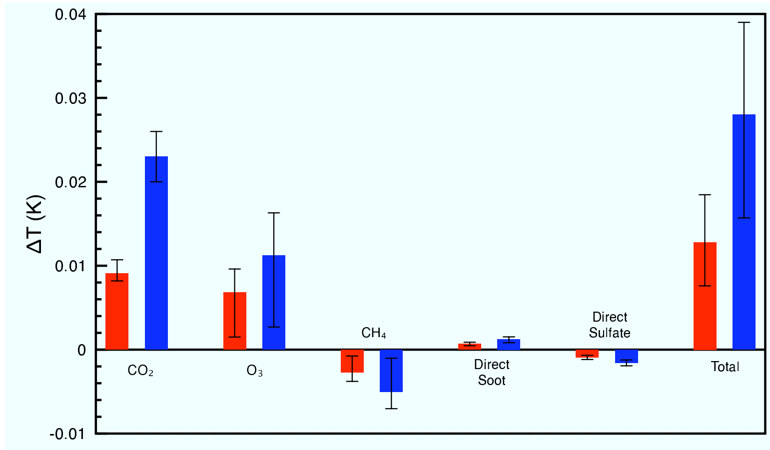

Figure 24: Surface temperature changes for different forcings by global aviation in 2002 (red) and 2025 (blue), averaged over the year, compared to scenario without aviation.

given in [IPCC 99] of 0.023 for the lowest scenario (Fc1). This can be attributed to several factors:

- AERO2k have supposed a slower increase as [IPCC 99] in distance flown and more strignent emission limitations for NO_x.(see [Eyers 04])
- The low climate senstivity of the model used
- The fact that the AERO2k data does not contain military aviation.

On the same figure we can also see that on a global mean the increase due to carbon dioxide released by aviation is about two times greater than that by ozone. Furhermore the increases of all factors will have doubled approximately in 2025 compared to 2002, which in in accordance with the fact that the aircraft movements have been predicted to double in that time period. As was mentioned in the introduction only the increase in green house gases and aerosols was modeled with this 1DRCM, However as figure 7 suggest, forcings from perturbation of cirrus due to aviation are probably the most important factor.

5.3.2 Surface Temperature Change due to Aviation in Europe

As on figure 24 we have given the surface temperature increase due to aviation for 2002 and 2025, but this time we restricted ourself to the European domain. For the well-mixed greenhouse gases, CO_2 and CH_4 the obtained values are nearly equivalent to the ones obtained on a global scale, as their concentrations in the air are the same. However for the ozone, whose concentrations are approximatly 5 times higher over Europe than on a global mean, due to the higher traffic density, the temperature increase is nearly 3 times higher in Europe than on a global mean. Thus ozone is the most important factor in Europe, apart from contrails and changes in cirrus clouds, which have not been assessed in this study. It is important to note that this strong local increase in surface temperature does not include any feedback parameters, such as an increase in the meriodinal energy transport. This can be compared to the existence of the meriodinal transport of energy which is needed to transport the excess of energy from the equator (where mean solar

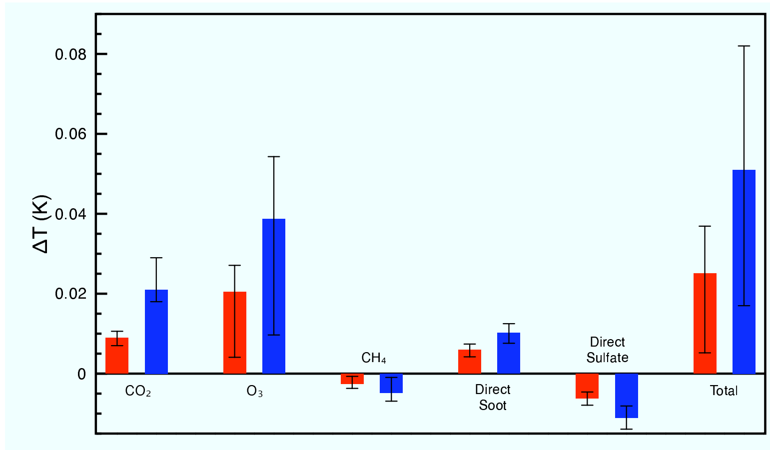

Figure 25: Surface temperature changes for different forcings by aviation in Europe in 2002 (red) and 2025 (blue), averaged over the year, compared to scenario without aviation.

radiation is greatest) to the pole. We thus see that the climate systems can redistribute energy inhomogeneities.

We have also assessed the average surface temperature changes January as well as for June, as shown in figure 27. For carbon dioxide and methane there are no changes in the concentations for the different months and the changes observed are due to the fact that the vertical temperature is different for these months. However for the ozone perturbation there is a seasonal change due to different traffic intensities which is shown in figure 26. We see that the perturbation is biggest in July, whereas the January perturbation is only slightly smaller than the annual mean one.

Figure 27 gives the surface temperature changes for the different seasons. We see that for the perturbations considered here, the total surface temperature increase is biggest in July, due to the fact that traffic is strongest in this season, and smallest in January.

Figure 28, gives the same seasonal variations in the surface temperature change for different seasons, but this time for the prediction year 2025. We can see the same pattern of seasonal change as for 2002, but all the changes are about twice as big, due to the predicted doubling of fuel use.

Theses seasonal variations should only be regarded as a first order of magnitude, because the model was initially thought to run on a yearly base, and the seasonal variation is thus very simple. A regional model with a more sophisticated seasonal cycle needs to be used to get more reliable results.

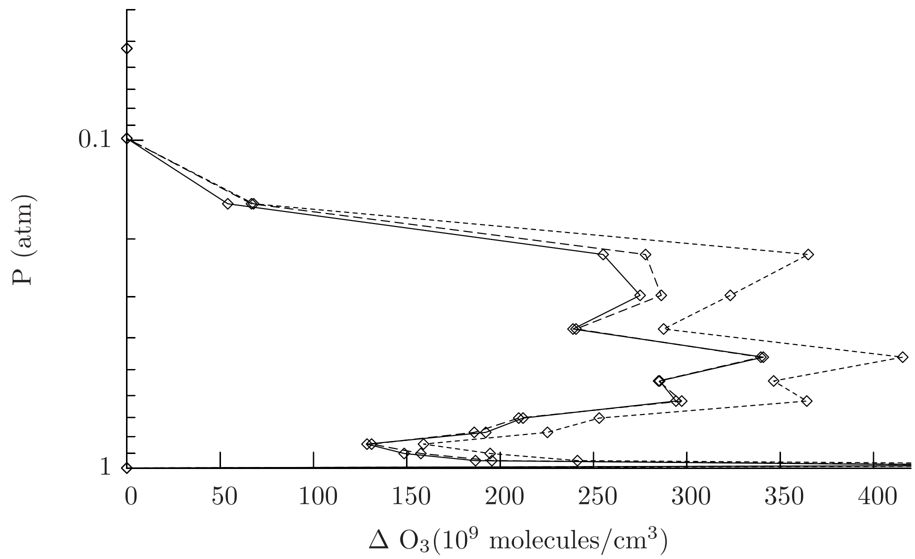

Figure 26: Ozone perturbation for different seasons. Annual mean (continuous line), January (small dashed line) and July (brad dashed line)

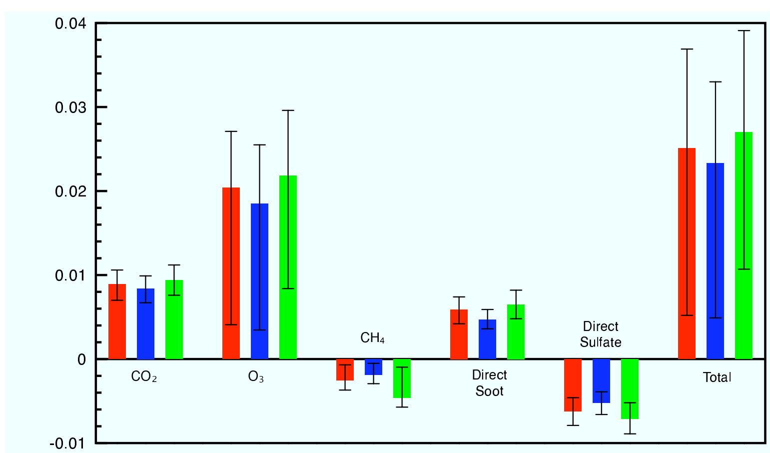

Figure 27: Surface temperature changes for different forcings by aviation in Europe in 2002, compared to scenario without aviation. The red bars indicate the changes averaged over the year, the blue ones for January and the green ones for July

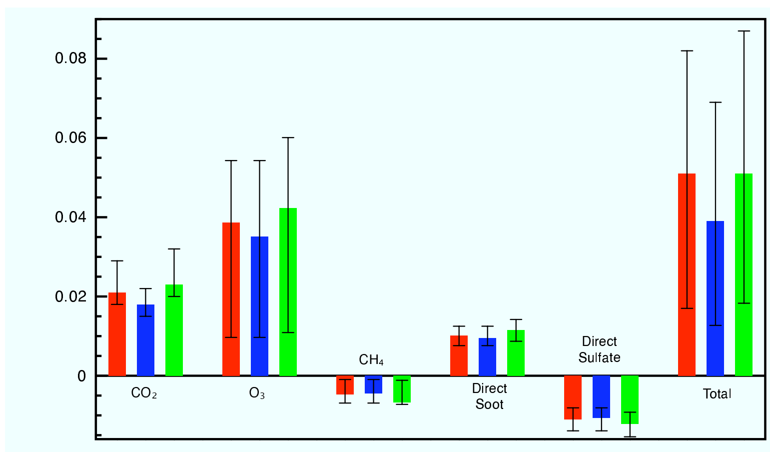

Figure 28: Surface temperature changes for different forcings by aviation in Europe in 2025, compared to scenario without aviation. The red bars indicate the changes averaged over the year, the blue bars for January and the green bars for July. (Note different vertical scale compared to figure 27)

OUTLOOK

These final results show the different impacts that have been accessed in this thesis. Ozone has the greatest impact in Europe, due to the high concentrations of flights in this region. But as has been explained on several occasions, the impact of cloud changes has not been calculated with this one dimensional model. As the coverage of potential contrail cover is not saturated, the impact of aircraft on clouds is estimated to be linearly correlated to air traffic density. This indicates that the forcing due to cirrus clouds should be the most important factor over Europe.

From figure 18 it would be tempting to conclude that flying higher or lower would reduce the impact of ozone, as was already discussed in section 2.2.3. As for technical reasons to fly higher would require new aircraft, some scientists have suggested to limit the maximal flight altitudes. Due to the higher density of the air at lower altitudes this increases fuel consumption and thus CO_2 emissions. But due to the lower impact of ozone and also cloud related impacts the overall instant impact is reduced.

However in order to get a more detailed estimation of this impact a 3D model including feedbacks needs to be used. As I have already discussed in section 5.1.1 if these feedbacks are included the maximum flattens out, and thus the impact of ozone will stay constant when airplanes are flying lower.

The final results also show the importance of the integration over time and space that was explained in section 1.4. Effectively we see that compared to the surface temperature on a global mean (figure 24) the increase in Europe (figure 25) is nearly twice as high in 2002 and 1.8[57] times as high in 2025. These factors will be higher when all the factors will be considered. This shows the importance of a climate index that includes all the regional and temporal variability of emissions to be used in an emission trading scheme for aviation.

We can thus conclude that even with this simple model some important features of the climate impact of aviation can be evaluated, but further work needs to be done. It will primarily necessary to calculate the impact of cirrus cloud changes due to aviation, and use a three dimensional regional model including climate feedbacks to get a more detailed view of the climate impacts in Europe and their seasonal variability. Finally it will be important to evaluate the strength and weaknesses of different climate indexes when they are applied to climate change due to aviation.

[57] This lower factor is due to the supposed in lower NO_x emission index during the forecast period.

Appendix A
Physics of atmospheric diffusion

In this Appendix we will give an overview of the physics involved in the diffusion processes that take place in the atmosphere. We will begin by molecular diffusion, followed by scattering of the solar radiation by clouds and aerosols, where we explain how Mie's theory may be applied to the particles in suspension in the atmosphere. Finally we will discuss the impact of absorption by aerosols and clouds on the solar and infrared radiation.

A.1 Molecular diffusion

Before entering into the details of diffusion in the atmosphere let us recall some notions of classical physics. If radiation passes form one medium to another whose index of refraction is different, there is a deviation of the luminous ray (the ray is said to be *refracted*). When the variation of index happens on a small length compared to the wavelength, a certain amount of radiation is furthermore returned to the first medium in a preferred direction: in this case there is *reflection*.

If the radiation passes through holes in a plate or hits obstacles whose dimensions are of the same order of magnitude than the wavelength, the radiation is again deviated but in a certain number of privileged directions. This is the phenomena of *diffraction*. Finally when the radiation is reflected in all directions by the irregularities of a surface that are not uniform and whose dimensions are of the order of magnitude of the wavelength, we are in presence of a phenomena of *scattering*.

The incident solar radiation is not only scattered by the aerosols contained in the atmosphere whose impact will be discussed in section A.2, but also by the molecules composing the air. This scattering is the main cause of the diurnal luminosity of the sky, and only becomes affective below an altitude of 50 km (above of this altitude the density of the air is too low). As the dimensions of the molecules are of the order of magnitude of the wavelength, Rayleigh scattering may be applied. This means that:

- the scattered intensity is proportional to λ^{-4}.
- the scattering coefficient can be approximated by:

$$k_\lambda^{\mathrm{sm}}\rho = \frac{32\,\pi^3}{3N}\,(n-1)^2\,\frac{1}{\lambda^4}, \tag{27}$$

where ρ is the density of the air, N the number of molecules per unit volume and n the refraction index of the gas. To get the exact formula, we would have to include a correction factor that is very close close to unity and accounts for the anisotropy of the molecules. Furthermore the attenuation coefficient has been shown to be proportional to $\lambda^{-4.09}$. Equation (27) shows that in the visible spectrum the blue light is more scattered than the red one, which explains that the sky appears to be blue.

A.2 Scattering of incoming Radiation by Aerosols and Clouds

As was mentioned in the preceding section scattering also takes place for aerosols suspended in the atmosphere. Their dimensions vary between a few millimeters and and a few tenth of microns, and this big range implies that according to their dimensions they may diffract light differently.

We can say that the optical properties of aerosols depend on two parameters:

- their refraction index, which is in general complex, and depends on the chemical properties of the aerosols,
- and the factor ϕ which compares the diameter of the particle (supposed to be spherical) to the wavelength of the incident light:

$$\phi = \frac{d}{\lambda} = \frac{2\pi r}{\lambda},$$

where, d is the diameter of the particle, λ the wavelength of the radiation and r the radius of the particle.

The general theory giving the scattering due to aerosols is Mie's theory, which can be derived from Maxwell's equations. In all generality Mie's theory gives the scattering coefficient to be:

$$k_\lambda^{\mathrm{sa}}\,\rho = K_d\left(\frac{d}{\lambda}, n\right) N\,\frac{\pi d^2}{4},$$

where $K_d(\frac{d}{\lambda}, n)$ is the dimensionless factor of effective scattering, function of ϕ and the refraction index of the gas n, ρ is the density of the gas in g·cm^{-3} and N is the number of particles per unit of volume, expressed in cm^{-3}.

However as a function of the the parameter ϕ more simple approximations can be used:

- If $\phi \ll 1$ (i.e. $d \ll \lambda$), it can be shown that we have a pure diffraction, like for gas molecules. Each particle emits a more or less spherical wave, with the same wavelength λ as the incoming wave (Rayleigh scattering). The diffused energy is proportional to λ^{-4} and the scattering coefficient for the aerosols has the same proportionality. The scattering coefficient (k_λ^{sa}) for these aerosols is:

$$k_\lambda^{\mathrm{sa}} \propto \frac{1}{\lambda^4}.$$

- if $\phi \gg 1$ (i.e. $d \gg \lambda$), the scattered radiation can be obtained by applying the laws of optics, corrected by those of diffraction. In the atmosphere the only particles of theses size are the droplets of water, and ice particles (i.e. precipitation and clouds). The index of refraction is varying very little with wavenumber for water and ice and this remains true also for the scattering by clouds and precipitation, at least for the visible and the ultraviolet spectra. Thus for water droplets and ice particles we have:

$$k_\lambda^{\mathrm{sa}} \perp \lambda.$$

- if $\phi \sim 1$ (i.e. $d \sim \lambda$) we have to apply Mie's theory, based on Maxwell equations. We then find that scattering index of the aerosol has a oscillating spectrum, implying that the diffused light can have any color.

  In general the scattering coefficient is supposed to have the following form:

  $$k_\lambda^{\mathrm{sa}} \propto \frac{\beta}{\lambda^\alpha},$$

  where β is called the blur parameter and is linked to the number of molecules ($0.05 \leq \beta \leq 0.20$). It is decreasing with altitude and has maximal values in industrial and urban regions due to the high anthropogenic concentrations of aerosols in this regions. α can take values between 0 and 4 depending on the type of aerosols considered. It represents the distribution of the numbers of particles. It is grows when the number of small particles is going up. In an atmosphere containing a very high number of aerosols, α is very close to zero.

To conclude we can thus write for the diffraction index of the solar spectrum, as a function of the dimension d of the aerosols:

$$\begin{array}{ll} d = 0.2\mu\mathrm{m} & k_\lambda^{\mathrm{sa}} \propto \frac{1}{\lambda^4}, \\ 1 \leq d \leq 4\mu\mathrm{m} & k_\lambda^{\mathrm{sa}} \propto \frac{\beta}{\lambda^\alpha}, \\ d > 16\mu\mathrm{m} & k_\lambda^{\mathrm{sa}} \perp \lambda. \end{array}$$

A.3 Absorption of Radiation by Aerosols and Clouds

The absorption of aerosols and cloud droplets is linked to the imaginary art of the refraction index n. Knowing the characteristics of a type of aerosols permits to calculate their absorption coefficient.

It can be shown that for sulfate particles the absorption is negligible, and thus they mainly scatter radiation according to Mie's theory. Whereas soot particles absorb mainly the incoming radiation and there is virtually no scattering.

Water and ice, that compose the clouds are nearly transparent in the near ultraviolet as well as in the visible spectrum. However clouds are very absorbent for infrared radiation above a wavelength of 2μm. This implies that they have very little effect on the incoming solar radiation because its fraction of energy above 2μm is very small. However the clouds act as a black body for the infrared radiation emitted by the surface of the Earth.

We thus see that clouds have two opposite effects on climate. On the one hand they reflect some of the incoming solar radiation by scattering, thus inducing a decrease of surface temperature, and on the other hand they reflect some of the outgoing infrared radiation from the Earth surface.

For cirrus cloud it can be shown that due to the fact that they are very thin the reflection of incoming radiation is small and due to their very low temperature they reflect a lot of infrared radiation from the surface. Their total effect is thus in general to warm the Earth's surface.

Appendix B
Techology of AIRCRAFT ENGINES

In this appendix we will give a brief overview of the technology of aircraft engines, the components of which play an important role in the climate impact of aviation, due to the fact that gases perturbations climate are formed in the engines. (for further details refer to [IPCC 99] chapter 7 pp.216)

B.1 Basic Engine Technology

Modern commercial aircraft nearly all use gas turbine engines. Many short-haul aircrafts still use theses gas-turbines to drive a propeller in so-called trubo-prop form. Planes equipped with theses types of engines are mainly used on short routes where cruise speeds are less important. Nevertheless many operators tend to acquire newer, more silent small jet planes, mainly to increase passenger comfort and their image. During the last decade, these have overtaken a huge part of the former market dominated by turbo-prop driven aircrafts [Mozdzanowska 03].

Today all of the medium- and long-hauled flights are operated by aircrafts equipped with bypass jet engines. A schematic description is shown by figure 29 (c). We can distinguish a core of the basic gas turbine, which is build up of three main parts: the compressor used to increase the energy of the air (by raising the pressure and the temperature), the combustor in which fuel is burned (this increases the temperature of the air further), and finally the turbine used to extract enough energy from the compressed gas to drive the compressor. A further low pressure turbine is then used to drive the fan at the front of the engine, which produces the bypass jet that is mainly used to propel the vehicle. Engineers try to develop engines which have a higher and higher bypass ratio[58] to increase overall efficiency of the engines.

A key element of the engine is the combustor, where the high pressured air enters with a relatively high velocity. The air is first carefully decelerated to minimize pressure losses, then forced into the combustion chamber, where fuel is added. The combustion chamber is designed to allow space and time for the fuel to mix with the air and burn efficiently before entering the turbine stages. As the detailed design of the combustion chamber has an impact on the completion of the chemical reactions involved, the combustor plays a key role in determining the emissions of secondary combustion products, and therefore the impact of aircraft on climate.

[58] this is the ratio of the fan bypass airflow and the engine core flow

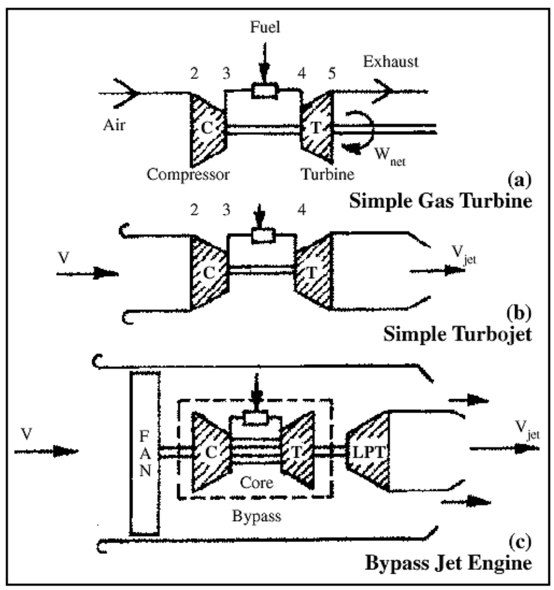

Figure 29: Gas turbine schematics (taken from [IPCC 99])

BIBLIOGRAPHY

[Berntsen 03] T. K. Berntsen, M. Gauss, I. S. A. Isaksen, V. Grewe, R. Sausen, G. Pitari, E. Mansini, E. Meijer & D. Hauglustaine. *Sources of NOx at cruise altitudes: Implications for poredictions of ozone and mathane perturbations due to NOx from aircraft.* Proceddings of the AAC-Conference, June30 to July 3, 2003, Fridrichshafen, Germany, pages 190–196, 2003.

[Brasseur 98] G.P. Brasseur, R.A. Vox, D. Hauglustaine, I. Isaksen, J. Leliveld, D.H. Lister, R. Sausen, U. Schumann, A. Wahner & P. Wiesen. *European scientific assessment of the atmospheric effects of aircraft emissions.* Atmospheric Environment, vol. 32, no. 13, pages 2329–2418, 1998.

[Eyers 04] C.J. Eyers, P. Norman, J. Middel, M. Plohr, S. Michot & K. Atkinson. *AERO2k Global Aviation Emissions Inventories for* 2002 *and* 2025, 2004.

[Gettelman 99] A. Gettelman & S. L. Baughcum. *Direct deposition of subsonic aircraft emissions into the stratosphere.* Journal of Geophysical Research, vol. 104, pages 8317–8328, 1999.

[Hansen 97] J. Hansen, M. Sato & R. Ruedy. *Radiative forcing and climate response.* Journal of Geophysical Research, vol. 102, pages 6831–6864, 1997.

[Holton 95] J.R. Holton, P.H. Hansen, M.E. McIntyre, A.R. Douglas, R.B. Rood & L. Pfister. *Stratosphere - troposphere exchange.* Geophysical Research Letters, vol. 24, pages 1335–1338, 1995.

[IPCC 99] IPCC, Joyce E. Penner, David H. Lister, David J. Griggs, David J. Dokken & Mack McFarland, editors. Aviation and the global atmosphere. Cambridge University Press, Cambridge, United Kingdom and New York, NY, USA, 1999.

[IPCC 01] IPCC, J.T. Houghton, Y. Ding, D.J. Griggs, M. Noguer, P.J. von der Linden, X. Dai, K. Maskell & C.A. Johnson, editors. Climate change 2001: The scientific basis. contribution of working group i to the third assessment report of the intergovernmental panel on climate change. Cambridge University Press, Cambridge, United Kingdom and New York, NY, USA, 2001.

[Isaksen 04] I. S. A. Isaksen & e. al. *The EU project TRADEOFF - Aircraft emissions: Contributions of various climate compounds to changes in composition and radiative forcing - tradeoff to reduce atmospheric impact, Project Final report.* Science, page 158, 2004.

[Kiendler 02] A. Kiendler & F. Arnold. *First Composition measurements of positive chemiions in aircraft jet engine exhaust: detection of numerous ion species containing organic compounds.* Atmos. Environm., vol. 36, pages 2979 – 2984, 2002.

[Lacis 74] A. A. Lacis & J. Hansen. *A Parameterization for the Absorption of Solar Radiation in the Earth's Atmosphere.* Journal of Atmospheric Sciences, vol. 31, pages 118–133, January 1974.

[Lohmann 02] U. Lohmann & B. Karcher. *First interactive simulations of cirrus clouds formed by homogeneous freezing in the ECHAM general circulation model.* J. Geophys Res., vol. 107(D10), no. 4105, 2002.

[MacKay 91] R.M. MacKay & M.A.K. Khalil. *Theory and Development of a one Dimensional Time dependent Radiative Convective Climate Model.* Chemopshere, vol. 22, no. 3–4, pages 393–417, 1991.

[Marquart 03] S. Marquart, M. Ponater, F. Mager & R. Sausen. *Future Development of Contrail Cover, Optical Depth and Radiative focring: Impacts of Increasing Air Traffic and Climate change.* J. Climate, vol. 16, no. 17, 2003.

[Minnis 99] P. Minnis, U. Schumann, D.R. Doelling, K.M. Gierens & D. Fahey. *Global distribution of contrail radiative forcing.* Geophyscial Research Letters, vol. 26, pages 1853–1856, 1999.

[Mozdzanowska 03] A. Mozdzanowska, R. J. Hansman, J. Histon & D. Delahaye. *Emergence Of Regional Jets And The Implications On Air Traffic Management.* 5th Eurocontrol / FAA ATM R&D Seminar, 23rd - 27th June 2003.

[Myhre 98] G. Myhre, F. Storndal, K. Restad & I Isaksen. *Estimation of the direct radiative forcing due to sulfate and soot aerosols.* Journal of Climate, vol. 8, pages 57–80, 1998.

[Myhre 01] G. Myhre & F. Stordal. *On the tradeoff of the solar and thermal infrared radiative impact of contrails.* Geophysical Research Letters, vol. 28, pages 3119–3122, 2001.

[Ponater 02] M. Ponater, S. Marquart & R. Sausen. *Contrails in a comprehensive global climate model: parameterisation and radiative forcing results.* J. Geophys. Res., vol. 107(D13), no. 4164, page 158, 2002.

[Prather 94] M.J. Prather. *Lifetimes and eigenstates in atmospheric chemistry.* Geophysical Research Letters, vol. 21, pages 801–804, 1994.

[Russell 97] P. B. Russell, S. A. Kinne & R. W. Bergstrom. *Aerosol climate effects: Local radiative forcing and column closure experiments.* Journal of Geophysical Research, vol. 102, pages 9397–9408, 1997.

[Sausen 05] R. Sausen, Isaksen, I, Grewe, V, Hauglustaine, D, Lee, D, Myhre, G, Köhler, M. O, Pitari, G, Schumann, U, Stordal, F, Zerefos & C. *Aviation Radiative forcing in 2000: An Update on IPCC (1999).* Meteorol. Z., vol. 14, pages 555 – 561, 2005.

[Schumann 96] U. Schumann, J. Ström, R. Busen, R. Baumann, K. Gierens, M. Krautstrunk, F. P. Schröder & J. Stingl. *In situ observations of particles in jet aircraft exhausts and contrails for different sulfur-containing fuels.* Journal of Geophysical Research, vol. 101, pages 6853–6870, 1996.

[Schumann 03] U. Schumann. *Aviation, Atmosphere and Climate- What has been learned.* pages 349–355, 2003.

[Sellers 65] W. D. Sellers. Physical climatoloy. The Universtiy of Chicago Press, Chicago & London, 1965.

[Shine 03] K. P. Shine, J. S. Fuglestvedt & N. Stuber. *An alternative to the Global Warming Potential for comparing climate impacts of emissions of greenhouse gases.* CICERO, vol. 2003:03, page 21pp, 2003.

[Stordal 05] F. Stordal, G. Myhre, E.J.G. Stordal, W.B. Rossow, D.S. Lee, D.W. Arlander & T. Svendby. *Is there a trend in cirrus cloud cover due to aircraft traffic?* Atmospheric chemistry and Physics, vol. 5, pages 2155–2162, 2005.

[Tonneau 02] R. Tonneau. Sensibilité des projections climatiques à la présence de suies et d'aérosols soufrés dans l'atmopshère. Master's thesis, Universtié Catholique de Louvain-la-Neuve, 2001-2002.

[Travis 02] D. J. Travis, A. M. Carleton & R. G. Lauritsen. *Contrails reduce daily temperature range.* Nature, vol. 418, pages 601 – 601, 2002.

[UNFCCC 05] UNFCCC. *Compilation of Data on Emissions from International Aviation.* Subsidary Body for Scientific and Technolgical Advice, pages Twenty–second session, 19–27 May 2005.

[Vancassel 04] X. Vancassel, A. Sorokin, P. Mirabel, A. Petzold & C. Wilson. *Volatile particles formation during PartEmis: a modelling study.* Atmos. Chem. Phys., vol. 4, pages 439 – 447, 2004.

[Wauben 97] W.M.F. Wauben, P.F.J. van Velthoven & H. Kelder. *A 3D chemistry transport model study of changes in atmospheric ozone due to aircraft NO_x emissions.* Atmospheric Environment, vol. 31, pages 1819–1836, 1997.

[Williams 02] V. Williams, R. B. Noland & R. Toumi. *Reducing The Climate Change Impact of Aviation By Restricting Cruise Altitudes.* EGS XXVII General Assembly, Nice, 21-26 April 2002, abstract #1331, vol. 27, page 1331, 2002.

[Wit 04] Ron Wit, Bettina Kampman, Bart Boon, Peter van Velthoven, Ernst Meijer, Jos Olivier & David S. Lee. *Climate impacts from international aviation and shipping.* 2004.

[WMO 99] WMO. Scientific assessment of ozone depletion: 1998, global ozone research and monitoring project. World Meteorogical Organization, Geneva, Switzerland, 1999.

[Zerefos 03] C.S. Zerefos, K. Elefthratos, D.S. Balis, P. Zanis, G. Tselioudis & C. Meleti. *Evidence of impact of aviation on cirrus cloud formation.* Atmospheric chemistry and Physics, vol. 3, pages 1633–1644, 2003.

FURTHER READING

[Delmas 05] R. Delmas, G. Mégie & V. H. Peuch. Physique et chimie de l'atmosphère. Editions belin edition, 2005.

[Forster 06] P. M. Forster, K. P. Shine & N. Stuber. *It is premature to include non-CO_2 effects of aviation in emission trading schemes.* Atmospheric Environment, vol. 40, pages 1117–1121, 2006.

[Gauss 03] M. Gauss, I. Isaksen, V. Grewe, M. Köhler, D. Hauglustaine & D. Lee. *Impact of Aircraft NOx Emissions: Effects of Changing the Flight Altitude.* Proceedings of the AAC-Conference, pages 122–127, June 30 to July 3 2003.

[Gierens 99] K. Gierens, R. Sausen & U. Schumann. *A Diagnostic Study of the Global Distribution of Contrails Part II: Future Air Traffic Scenarios.* Theoretical and Applied Climatology, vol. 63, pages 1–9, 1999.

[Gössling 03] S. Gössling. *The Importance of Aviation for Tourism ? Status and Trends.* Proceedings of the AAC-Conference, pages 156–161, June 30 to July 3 2003.

[Grewe 03] V. Grewe. *Lightning NO_x emissions and the impact on the effect of aircraft emissions — Results from the EU-Project TRADEOFF.* Proceedings of the AAC-Conference, June 30 to July 3 2003.

[Hendricks 04] J. Hendricks, B. Kärcher, A. Döpelheuer, J. Feichter, U. Lohmann & D. Baumgardner. *Simulating the global atmospheric black carbon cycle: a revisit to the contribution of aircraft emissions.* Atmospheric Chemistry & Physics Discussions, vol. 4, pages 3485–3533, 2004.

[H.Jäger 98] H.Jäger, V.Freudenthaler & F. Homburg. *Remote sensing of optical depth of aerosols and clouds related to air traffic.* Atmopsheric Environment, vol. 32, no. 18, pages 3123–3127, 1998.

[Kärcher 03] B. Kärcher & J. Ström. *The roles of dynamical variability and aerosols in cirrus cloud formation.* Atmospheric Chemistry & Physics Discussions, vol. 3, pages 1415–1451, 2003.

[Köhler 03] M. O. Köhler, H. L. Rogers & J. A. Pyle. *Modelling the Impact of Subsonic Aircraft Emissions on Ozone: Future Changes and the Impact of Cruise Altitude Perturbations.* Proceedings of the AAC-Conference, pages 173–177, June 30 to July 3 2003.

[Kraabøl 02] A. G. Kraabøl, T. K. Berntsen, J. K. Sundet & F. Stordal. *Impacts of NO_x emissions from subsonic aircraft in a global three-dimensional chemistry transport model including plume processes.* Journal of Geophysical Research (Atmospheres), vol. 107, no. D22, pages 22–+, November 2002.

[**Lacis 90**] A. A. Lacis, D. J. Wuebbles & J. A. Logan. *Radiative forcing of climate by changes in the vertical distribution of ozone*. Journal of Geophysical Research, vol. 95, pages 9971–9981, June 1990.

[**Meerkötter 99**] R. Meerkötter, U. Schumann, D. R. Doelling, P. Minnis, T. Nakajima & Y. Tsushima. *Radiative forcing by contrails*. Annales Geophysicae, vol. 17, pages 1080–1094, August 1999.

[**Meijer 03**] E. W. Meijer, P. F. J. van Velthoven, A. Segers, B. Bregman & D. Brunner. *Improved Mass Fluxes in a Global Chemistry-Transport Model: Implications for Upper-Tropospheric Chemistry*. Proceedings of the AAC-Conference, pages 128–133, June 30 to July 3 2003.

[**Meyer 02**] R. Meyer, H. Mannstein, R. Meerkötter, U. Schumann & P. Wendling. *Regional radiative forcing by line-shaped contrails derived from satellite data*. Journal of Geophysical Research (Atmospheres), vol. 107, no. D10, pages 17–+, May 2002.

[**Minnis 03**] P. Minnis, J. K. Ayers, M. L. Nordeen & S. P. Weaver. *Contrail Frequency over the United States from Surface Observations*. Journal of Climate, vol. 16, pages 3447–3462, November 2003.

[**Ramanathan 78**] V. Ramanathan & Jr. J.A. Coakley. *Climate Modeling Through Radiative Convective Models*. Reviews of Geophysics and Space Physics, vol. 16, no. 4, pages 465–489, 1978.

[**Rodriguez 03**] J. M. Rodriguez, J. A. Logan, D. A. Rotman, D. J. Bergmann, R. R. Friedl & D. E. Anderson. *Activities of NASA?s Global Modeling Initiative (GMI) in the Assessment of Subsonic Aircraft Impact*. Proceedings of the AAC-Conference, pages 134–139, June 30 to July 3 2003.

[**Sausen 98**] R. Sausen, K. Gierens, M. Ponater & U. Schumann. *A Diagnostic Study of the Global Distribution of Contrails Part I: Present Day Climate*. Theoretical and Applied Climatology, vol. 61, pages 127–141, 1998.

[**Schine 05**] K. P. Schine, T. K. Bernstesen ans J.S. Fuglestvedt & R. Sausen. *Scientific issues in the design of metrics for inclusion of oxides of nitrogen in global climate agreements*. Proc. Natl. Acad. Sci. USA, vol. 102, no. 44, pages 15768–15773, November 1 2005.

[**Schlager 97**] H. Schlager, P. Konopka, P. Schulte, U. Schumann, H. Ziereis, F. Arnold, M. Klemm, D. E. Hagen, P. D. Whitefield & J. Ovarlez. *In situ observations of air traffic emission signatures in the North Atlantic flight corridor*. Journal of Geophysical Research, vol. 102, pages 10739–10750, May 1997.

[**Schumann 05**] U. Schumann. *Formation, Prperties and Climatic Effets of Contrails*. Comptes Rendus Physique, 2005.

[**Spichtinger 03**] P. Spichtinger, K. Gierens & W. Read. *The global distribution of ice-supersaturated regions as seen by the Microwave Limb Sounder*. Quarterly Journal of the Royal Meteorological Society, vol. 129, pages 3391–3410, October 2003.

[Wyser 02] K. Wyser & W. O. Hirok. *Modeling Radiation Effects of Contrails with High Spatial Resolution.* Earth Sciences Centre, Göteborg University, pages 4 – pp, 2002.